

A thesis presented for the degree of
Master of Science

**Towards drought preparedness:
A microfluidic lab study to the process
of BioSealing**

Author
T.H.G. Fernhout

Supervisors
Prof. dr. R.J. Schotting
Dr. A. Raof

DECEMBER 10, 2020



Utrecht University

Department of Earth Sciences
ENVIRONMENTAL HYDROGEOLOGY GROUP

Abstract

The Province of Yunnan (People's Republic of China) is known for its severe droughts between November and April. The people living in this Province have to deal with serious water scarcity problems as a consequence. Especially the subsurface is unfavourable for (rain) water storage. The subsurface is built up of fractured bedrock below a few meters of soil. When rain is falling water filtrates into the soil and flows towards the fractures in the bedrock leaving the soil. This causes the groundwater to be unreachable for groundwater extraction.

The soil and groundwater are known to be enriched by many types of microorganisms. Especially the soil bacteria are potentially helpful to solve the water scarcity problem in the Province of Yunnan. By feeding the ambient bacteria in the soil with a nutrient solution a process called BioSealing can be triggered that causes the fractures in the bedrock to be clogged. This process involves biological and physical clogging. The combination of these clogging mechanisms potentially leads to permanent clogging of the fractures. Rain water that seeps into the soil can now be stored in the soil and be pumped up to use for different purposes.

This study assesses the rate and behaviour of the products of the BioSealing process on the pore scale. Besides, different experimental approaches are tried to identify the different components present in the groundwater.

A spectrophotometer is used to measure the optical density at 600 nm (OD600) of several groundwater samples. These measurements give a first impression for the presence of bacteria and other organic material in the groundwater. The main focus of this study is to simulate the biological clogging part of the BioSealing process. For the simulation of this part an open-microscope set-up is used. This set-up consists of a PDMS micromodel containing a thin section of a porous medium that has two inlet channels and one outlet channel. The groundwater and nutrition (Nutrolase) are separately injected with a syringe pump through the micromodel. Images are taken with a digital photo camera of the porous medium while injecting the fluids. Finally a Confocal Laser Scanning Microscope (CLSM) has been used to acquire more detailed images of the groundwater, Nutrolase and a mixture of both fluids to get a better view of the particles inside the fluids. Fluoresbrite has been added to a few samples to observe the bacteria even better.

The measurements of the optical density of the groundwater gave a minor proof of the presence of bacteria in the groundwater. The following open-microscope experiments showed that biological clogging needs at least several days to have significant impact on obstructing groundwater flow. The potential biomass had the tendency to occupy the air bubbles that unwillingly entered the micromodel. The biomass also became denser with time and eventually occupied the boundaries of the air bubbles. The confocal microscope images did show a clearer view on the content of the fluids, but did not clarify for the presence of bacteria.

Keywords: BioSealing, bacteria, CLSM, fluorescence, micromodel

Acknowledgements

First of all, I would like to thank my supervisors prof. dr. Ruud Schotting and dr. Amir Raoof of the Utrecht University (UU) for proposing me to do research on BioSealing and giving me advice for the execution of the research. I also want to thank all researchers of the Environmental Hydrogeology Group (UU) that helped me out with setting up and conducting the lab experiments. In specific Enno de Vries, dr. Hamed Aslannejad and dr. ing. Matthijs de Winter. I am also thankful to laboratory supervisor Thom Claessen who explained me how to work with the lab equipment and Jan Gerritse who provided me the fluids I needed.

Last, I want to thank my family for supporting me and putting me on the right track when I tended to lose it.

Contents

Abstract	i
1 Introduction	1
2 Theoretical background	6
2.1 Multiphase flow	6
2.2 Soil bacteria and growth development	9
2.2.1 Soil bacteria	9
2.2.2 Bacterial growth phases	10
2.2.3 Biomass formation	10
2.3 Bacterial identification methods	13
2.4 Clogging factor	16
3 Methods and materials	17
3.1 Spectrophotometry (OD600)	17
3.2 Open microscope set-up	17
3.2.1 Confocal Laser Scanning Microscope (CLSM)	19
3.3 Experiments	20
3.3.1 OD600	20
3.3.2 Micromodel experiments (Open microscope)	20
3.3.3 CLSM experiments	21
3.4 Solutions	22
3.4.1 Groundwater	22
3.4.2 Nutrolase	23
4 Results	24
4.1 OD600	24
4.2 Micromodel experiments (open microscope)	25
4.2.1 Experiment 1	25
4.2.2 Experiment 2	26
4.3 CLSM images	28
5 Discussion	29
5.1 OD600	29
5.2 Micromodel experiments (Open microscope)	29
5.2.1 Experiment 1	29
5.2.2 Experiment 2	31
5.3 CLSM images	32
6 Conclusions & Recommendations	33
A Appendix	35
A.1 Images - Experiment 1 & 2	35
A.2 CLSM images	43
References	51

List of Figures

1	Yunnan, China	1
2	Soil Map of Yunnan 2010 (FAO/UNESCO classifications)	2
3	Schematic diagram of the experimental set-up used by J.-W. Kim et al. (2010).	5
4	Capillary pressure-saturation relationship (Mayer, 2005).	7
5	Capillary pressure-saturation curve for a water-air system of medium-grained sand (Mayer, 2005).	7
6	Typical relative permeability curves for a two-phase system, k_{rw} represents the relative permeability for the wetting phase, k_{rnw} is the relative permeability for the non-wetting phase (Mayer, 2005).	8
7	Left circle diagram shows the percentage of the most dominant soil bacterial phylotypes (Top 511 phylotypes). Right circle diagram shows the percentage that these dominant phylotypes represent in a soil bacterial community. Bar graph: Relative abundance of some dominant bacterial phylotypes (Delgado-Baquerizo et al., 2018).	9
8	Bacterial growth curve (Maier et al., 2009).	10
9	Biofilm formation stages. (1) Reversible cell attachment. (2) Irreversible attachment of bacteria to surface by EPS secretion. (3) Formation of biofilm microcolonies. (4) Mature biofilm structure. (5) Detachment of cells from biofilm (Valiei, 2013).	11
10	Photomicrographs of <i>P. aeruginosa</i> going through the five stages (a-e) of biomass development when growing under continuous conditions on a glass substratum (Stoodley et al., 2002).	11
11	Fluorescence (Semwogerere and Weeks, 2005)	13
12	Commonly used stains for soil microbiological studies and their properties (Li et al., 2004).	14
13	bacteria stained with ethidium bromide in a silt loam soil inoculated with <i>E. Coli</i> (Li et al., 2003).	15
14	Projection image of 25 confocal serial sections (taken at 0.4 mm increments) (Li et al., 2003).	15
15	Open microscope set-up.	18
16	Digital representation of a PDMS micromodel.	18
17	Configuration of a confocal laser scanning microscope (Li et al., 2004).	19
18	Manual groundwater extraction, Utrecht Science Park.	22
19	Optical density (600 nm) of groundwater through time.	24
20	Pressure gradient development across micromodel (exp. 1).	26
21	Pressure gradient development across micromodel (exp. 2).	27
22	Experiment 1	35
22	Experiment 1	36
22	Experiment 1	37
22	Experiment 1	38
23	Experiment 2.	39
23	Experiment 2.	40
23	Experiment 2.	41
23	Experiment 2.	42
24	Groundwater.	43
25	Diluted Nutrolase.	44
26	Nutrolase	45

27	Samples stained with fluoresbrite observed at 405 nm(topleft image) and 488 nm(topright image). The left bottom image is a normal image.	46
27	Samples stained with fluoresbrite observed at 405 nm(topleft image) and 488 nm(topright image). The left bottom image is a normal image.	47
27	Samples stained with fluoresbrite observed at 405 nm(topleft image) and 488 nm(topright image). The left bottom image is a normal image.	48

List of Tables

1	Experiment specifications	20
2	Chemical composition of Nutrolase.	23
3	Optical density measurements (600 nm) of groundwater (GW).	24

1 Introduction

Water scarcity in Yunnan, China

Yunnan, a densely populated Province located in the South of China (Fig. 1), is prone to severe droughts. During drought period (November-April), the average daily precipitation is 0.93 mm and in total accounts for 16 % of the precipitation in the entire year. This amount of precipitation is far lower than the evaporation rate, leaving very little water behind in the soil (Ren et al., 2017). Especially a severe drought period during Spring 2010 brought more than 20 million people in short-age of drinking water in this region. This occurrence aroused public awareness and made aware that opposed to flood preparedness against sea level rise, drought preparedness is also necessary in certain areas like Yunnan ("*Crack sealing bacteria and multi usage bamboo*", EurOman Magazine (Spring 2012), p32-33).

As these droughts occur frequently and for a long duration, they have a huge impact on the agricultural production and drinking water availability for this region. Hereby negatively affecting the regional and national economy of China (Ren et al., 2017).

During the wet season (May-October) the soil is recharged by rain water, but the infiltrated water leaves the soil through cracks in the underlying bedrock. At the end of this season, no groundwater is left to be pumped up for agriculture and other purposes. Storage of water in large tanks or artificial lakes were insufficient to fulfill the water needs of the population in Yunnan. Researchers from the Dutch research institute Deltares developed a method called BioSealing to clog leakages in the sub-surface. Application of this method in the soil in Yunnan may clog the cracks in the bedrock leading to the storage of groundwater in the subsurface.



Figure 1: Yunnan, China

Yunnan soil

Knowing the type of soil can be useful to predict the behaviour of water flow into and through the soil in Yunnan. The major soil groups in this area are (Fig. 2): acrisols (34.44%) in Southern Yunnan, cambisols (25.12%) in Central Yunnan, luvisols (22.44%) in Northwest Yunnan, alisols (7.36%) in Southwest, Southeast and Northeast Yunnan and anthrosols (4.39%) dispersed over the whole

province. (Chen et al., 2019). The soil texture of these soils is typically clayey and therefore have a slow infiltration rate but a good water retention capacity (see article Soil Potential). The acrisols are part of the red earth soils, a group of soils that is relatively abundant in China. These soils are red due to their relatively high amount of Fe as other chemical elements are leached out. Besides they are nutrient deficit and acidic soils (Barton et al., 2004).

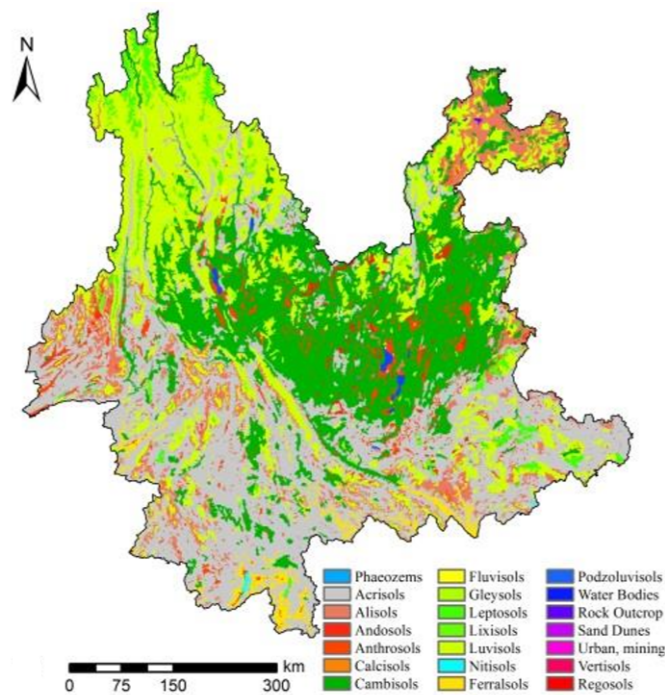


Figure 2: Soil Map of Yunnan 2010 (FAO/UNESCO classifications)

BioSealing

A well-known method for clogging a soil leakage is bioclogging. This process is based on the natural activity of bacteria in the soil. By adding nutrients at the appropriate location in the subsurface, biomass can grow and gather at or around the location of the leak or hole. This way a porous material or soil can be locally clogged e.g. for the management of groundwater flow at a contaminated site or an increase of the shear stress of the soil. Although to make this method work permanently, the nutrition has to be injected continuously. Without a constant nutrient injection, the produced biofilm can degrade and eventually disappear (Ivanov & Chu, 2008). A relatively identical method, called BioSealing, is based on the same principle as bioclogging. The application of this method is at an early stage, although it seems that this is a permanent solution as opposed to the temporal effect of bioclogging. The durability of BioSealing comes from the mechanical clogging by small mineral particles that aggregate as bridges at the location of the leak. As the soil in Yunnan is clayey, it is favourable for this to occur. Although the name of this method implies that it is a purely biological process, chemical and mechanical processes are also involved and have an important part in this mechanism (Blauw et al., 2009).

The hypothetical principle of BioSealing is postulated in five steps by Blauw et al. (2009):

- (1) Fermentation of the injected nutrients results in the production of organic acids. Fermentation may be accompanied by the formation of gas bubbles originating from butyric acid, which gives an unpleasant smell (E. E. van der hoek et al., (2003). After the nutrient injection, the gas formation was not observed anymore. On the other hand, Van Beek et al. (2007) did not observe any gas production.
- (2) The accompanying pH drop of the ground water causes small mineral particles ($<10\mu\text{m}$) to detach from larger grains. These particles are small enough to travel through the porous medium with the ongoing ground water flow. Meanwhile the population of bacteria grows exponentially. Most of the bacteria growth occurs at the leakage as the flow rate is at its maximum at this location.
- (3) By the addition of the nutrient solution, the extracellular polymeric substances (EPS) production of the bacteria also increases.
- (4) The formed EPS entraps the mobilized mineral particles at the leak.
- (5) Sealing of the leak is eventually achieved by the flocculation of these mineral particles by metal-ions present in the injected nutrient-solution or present in the groundwater. In particular chemical precipitation of iron sulphide reinforces the sealing process under anaerobic conditions (Farah et al., 2016). The production of an inorganic substance is the basis for the development of a durable clog, as organic substances degrade through time.

A similar sequence of processes occurring during BioSealing is confirmed by other studies (E. E. van der Hoek et al., 2003) (Van Beek et al., 2007) (van der Zon et al., 2012). Although the interactions between these processes still lacks full understanding.

The nutrient solution used by GeoDelft is called nutrolase. This substance is a sugar- and protein-rich rest product originating from the potato starch production. A list of its components can be find in Section 3.4.2.

Initially both aerobic and anaerobic bacteria are involved in the process of BioSealing. But after a while the aerobic bacteria will starve due to oxygen depletion according to a researcher of Deltares¹.

The main advantage of this method over other traditional methods is its self-localizing principle. A prerequisite for this to occur is the presence of a converging flow towards the leakage. Besides only environmentally-friendly solutions are used for this method as opposed to other traditional methods that make use of environmentally harmful substances (Blauw et al., 2009).

Previous studies

Several 2D bioclogging studies have successfully shown that this method works on this scale (Blauw et al., 2009). These experiments made use of a plane fracture apparatus (Ross et al., 2007) or a horizontal fracture in bedrock (Ross & Bickerton, 2002). Although durable clogging in 3D was not tested yet. Researchers from Deltares performed a pilot scale test to prove that bioclogging can be applied on a 3D scale as well with BioSealing (Blauw et al., 2009).

¹Private communication

Lab experimental studies (Liao et al., 2007) and a field experiment at a hydropower dam at Greifenstein, Austria (Blauw et al., 2009) have approved a significant decrease of the hydraulic conductivity and the soil permeability due to BioSealing. To achieve a durable clog, Blauw et al. (2009) concluded that a minimum time of three months after the last nutrient injection is needed. Van der Hoek et al. (2003) tested the clog durability by flushing a clog continuously with drinking water for 4-5 months, while no nutrition was injected without any leakage occurring.

Few experiments related to BioSealing have been conducted at the pore-scale so far. Studies that come close to this are done by Dupin & McCarty (2000), D.-S. Kim & Fogler (2000) and J.-W. Kim et al. (2010). D.-S. Kim & Fogler (2000) observed biomass evolution in a micromodel from nutrient-rich towards nutrient-poor conditions and distinguished four different biomass evolution phases. During phase 1 permeability decreases as a consequence of biomass formation. At the beginning of phase 2 the nutrient injection is stopped, while biomass continues to grow from the nutrients leftover. Subsequently when all nutrients are used, the amount of biomass declines due to sloughing of the ongoing water flow at phase 3. Finally at phase 4 the permeability stabilizes at some level. At this point the flow velocity is not large enough to shear off more biomass. This study also points out that initial biomass formation starts in the pore bodies and extends towards the pore throats of the pore network model.

D.-S. Kim & Fogler (2000) also studied biomass evolution in a micromodel, but focused on the effects of a high and low flow velocity and a high and low substrate concentration on biomass growth. A high flow velocity (7.50 mm/min) caused biomass to grow fast, but the biomass could easily be sloughed by shearing of the water flow. Applying a low flow velocity (1.25 mm/min) biomass grows slowly but densely and is therefore more resistant against shearing. Bioclogging with a relatively high substrate concentration (8000 ppm) also causes more densely formed biofilms to form as opposed to a low substrate concentration (1000 ppm). The ideal conditions for the most severe clogging is reached when a relatively low flow velocity (1.25 mm/min) and high substrate concentration (8000 ppm) are applied.

Nutrient solutions used during these experiments vary. Nutrient broth agar medium (J.-W. Kim et al., 2010) is a commonly used nutrient solution for cultivation of bacteria and production of biomass, but also acetate (Seifert & Engesgaard, 2007) (Dupin & McCarty, 2000) or a glucose solution can be applied (Thullner et al., 2002). Although the nutrient solutions used by the aforementioned studies have in common that they are high in carbon concentration. Besides, Ivanov & Chu (2008) state that a source with an excess of carbon over nitrogen (e.g. a protamylasse) should work for almost any bacteria to multiply and create biomass.

Besides the addition of a carbon source to the bacterial population, anaerobic conditions are also favourable for biomass growth and a significant decrease in saturated hydraulic conductivity as shown by Hand et al. (2008).

This study

As mentioned before the majority of the studies on biomass formation and BioSealing are conducted at macro scale. These studies give quantitative evidence for a decline in hydraulic conductivity of the porous medium, but lack in the understanding of this process at the pore scale. Therefore, the main purpose of this study is to investigate the process of BioSealing at the pore scale. How fast does the biomass grow? Which flow velocity is most effective? How does the biomass behave and distribute throughout the pore space? The experimental set-up and results of J.-W. Kim et al. (2010) will be used as a fundament for this study (Fig. 3). J.-W. Kim et al. (2010) used a nutrient broth agar medium to grow and image the bacteria with a confocal laser scanning microscope (CLSM) prior to the main micromodel experiment. A 40 times diluted solution of Nutrolase is optimal according to a BioSealing container experiment by Van Beek et al. (2007). This may vary according to the scale of the experiment.

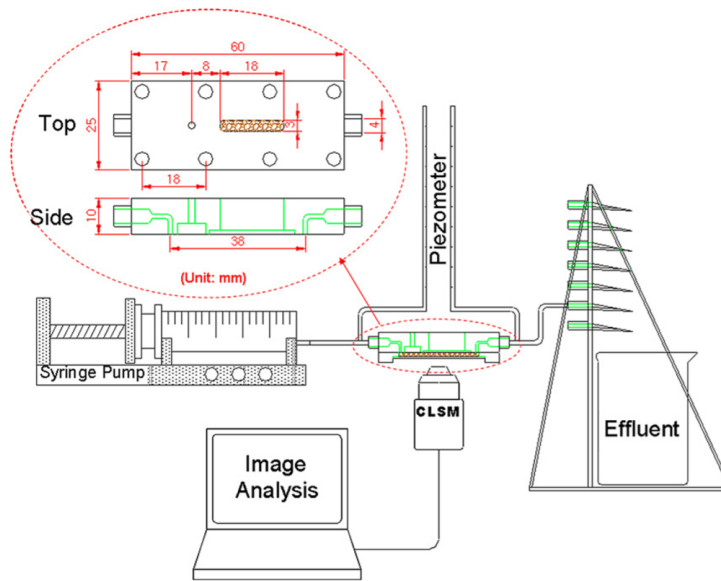


Figure 3: Schematic diagram of the experimental set-up used by J.-W. Kim et al. (2010).

The initial purpose of this study was to do a sensitivity analysis for several parameters (fluid flow rate, dilution nutrition) to observe its effect on the BioSealing process and to measure and discuss the accompanying clogging degree. Eventually the sensitivity analysis was not possible to execute due to circumstances. However the identification of the constituents of the fluids involved became also a part of this study. For this study, a porous medium made from a piece of PDMS (polydimethylsyloxane) is used, which is called a micromodel. This material, PDMS, is commonly used for among others biological and fluid flow experiments as its properties are favourable for these type of experiments (See Section 3.2 for a more detailed description). An open-microscope set-up using a digital photo camera and a confocal laser scanning microscope will be used for the lab experiments (see Section 3 for a detailed description of the experimental set-ups).

As a PDMS model is used for this study and the presence of metallic multivalent ions in the ground-water or nutrition is not verified, it is not possible to fully simulate the aforementioned steps of BioSealing. So mineral detachment and entrapment of these particles as well as permanent sealing is out the scope of this study. A basic beginning of the process will be simulated involving biological clogging with the nutrition (Nutrolase) used for BioSealing.

2 Theoretical background

2.1 Multiphase flow

When two or more immiscible phases (either liquid or gas) are present in a porous medium, they apply a force on each other at the interface between these phases. The imbalance between these forces causes the interface to be curved. The curvature tells which phase experiences a larger pressure, this is the non-wetting phase (e.g. air). The non-wetting phase typically experiences larger cohesive forces between molecules of the fluid than adhesive forces between the fluid and the grains of the porous medium. For the wetting phase (e.g. groundwater) the opposite counts. The capillary pressure that results from these pressures is a result of the pressure of the non-wetting phase minus the pressure of the wetting phase. At equilibrium conditions this pressure difference is balanced by the interfacial tension of the interface (Mayer, 2005). This phenomenon influences the dynamics of the fluid flow and the ability of for example groundwater through the porous medium.

Capillary pressure-saturation curve

Upscaling this phenomenon to the continuum scale, a relationship arises between the capillary pressure and the volumetric contents of the phases in the porous medium. As shown in Fig. 4 (the change of) the capillary pressure depends on the saturation level of the (non-)wetting phase. This graph is a typical graph for a specific porous medium and called the capillary pressure-saturation curve (P_cS-curve). It also shows that the way the capillary pressure of a porous medium changes depends on the initial wetting conditions and whether drainage or imbibition is applied. The primary drainage curve shows capillary pressure change when a fully saturated porous medium is drained. This curve is asymptotic as it continues infinitely towards a value called the irreducible saturation of the wetting phase. This is due to strong wetting phase attachment to the grain particles. As this porous medium is subsequently rewetted, the main imbibition curve is obtained. This curve ends at the residual saturation of the non-wetting phase. A primary imbibition curve can be obtained by wetting a dry porous medium.

A final characteristic of this graph is the displacement pressure. This pressure is needed to overcome before a fully saturated porous medium is drained.

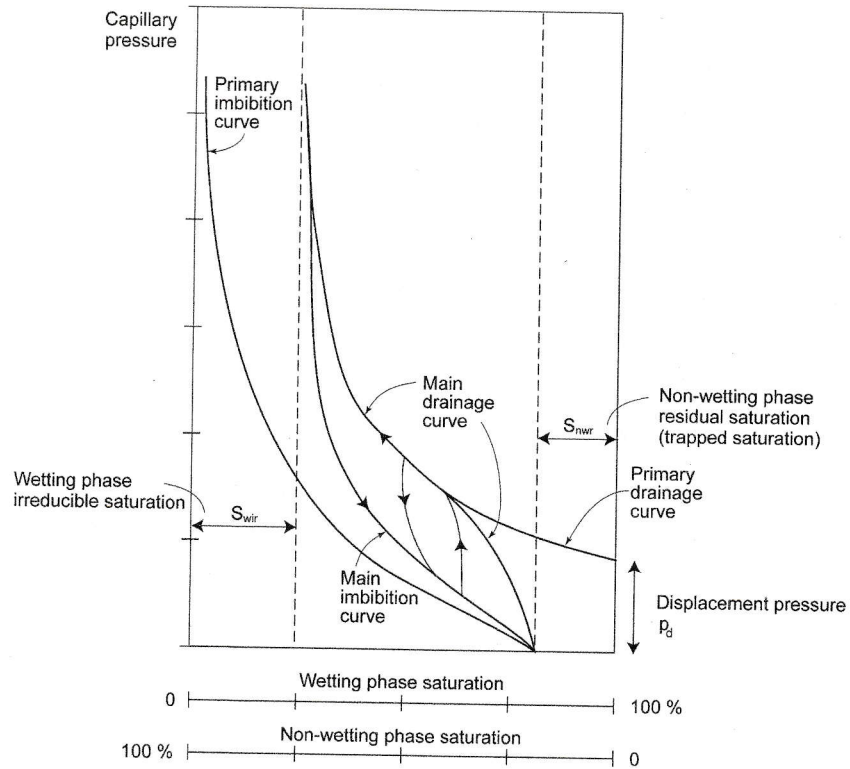


Figure 4: Capillary pressure-saturation relationship (Mayer, 2005).

According to the grain sizes of the grains of the porous media (0.3-0.9 mm) used in the experiments of this study, the porous medium represents a medium- to coarse-grained sand (grain-size range = 0.25 - 1 mm) (Blair & McPherson, 1999). Although the porosity of the porous medium (0.55) used for this study suggests that it represents a clayey soil. Fig. 5 shows a typical P_c - S -curve for a medium-grained sand.

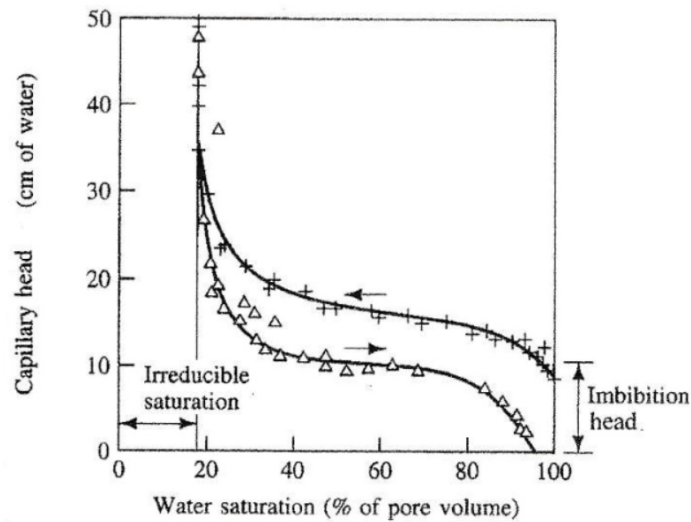


Figure 5: Capillary pressure-saturation curve for a water-air system of medium-grained sand (Mayer, 2005).

Relative permeability

In the presence of two or more phases in a porous medium, the permeability of either phases is smaller than the intrinsic permeability when only one phase is present. This concept is represented by the relative permeability, which is the ratio of the permeability of a phase at a given saturation to the intrinsic permeability. The relative permeability is a function of the saturation of the phase in the specific porous medium (Fig. 6). The shape of this graph also depends on the wettability of the phase with respect to the material of the porous medium. (Mayer, 2005)

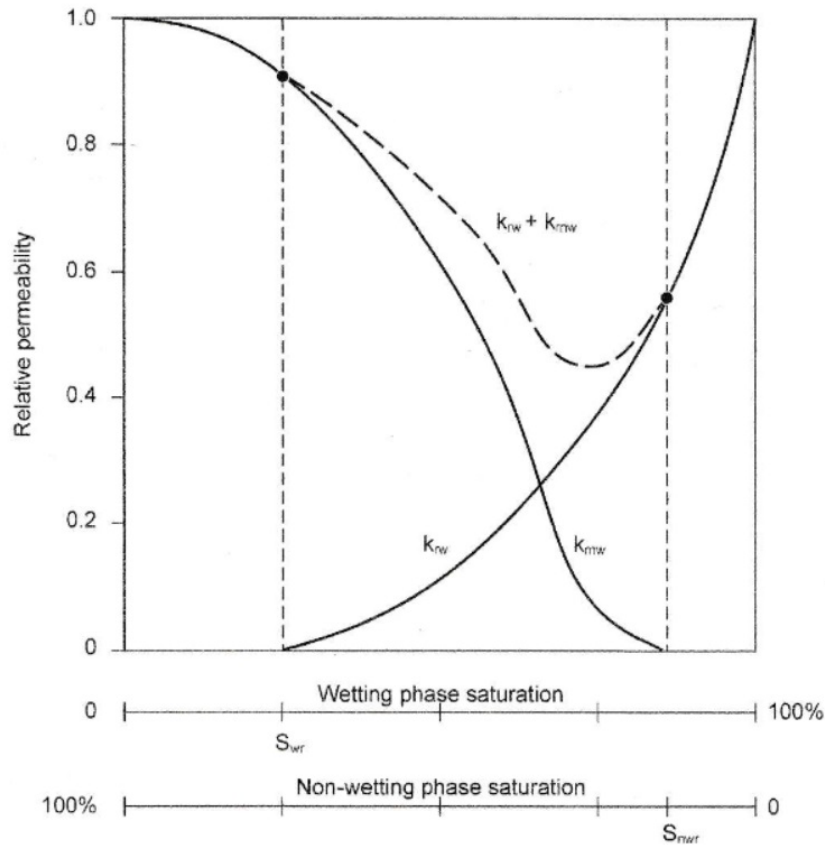


Figure 6: Typical relative permeability curves for a two-phase system, k_{rw} represents the relative permeability for the wetting phase, k_{rnw} is the relative permeability for the non-wetting phase (Mayer, 2005).

Beltrán et al. (2019) also studied the effect of a hydrophobic and hydrophilic surface of the grains on the relative permeability of the wetting phase. He concluded that the relative permeability increases when the hydrophobicity of the surface of the grains increases.

2.2 Soil bacteria and growth development

2.2.1 Soil bacteria

Soil microbiology

Relatively little is known about the biodiversity of microbiological life in the subsurface in comparison to the aboveground biodiversity, although knowledge about the spatial distribution and complexity of the soil biodiversity has been growing rapidly the past decades (Bardgett & Van Der Putten, 2014). A recent study by Delgado-Baquerizo et al. (2018) found that about 2% of all known bacterial phylotypes (=biological classification group based on observable traits) comprises for almost half of the global soil bacterial communities (Fig. 7). The main representatives of the 511 most dominant phylotypes are the proteobacteria and actinobacteria. They also found that the presence of a certain soil bacterial community can be related to the ecology of a region.

The increase of knowledge is partly due to the advancement in the identification methods of bacteria. A method that is currently applied is able to identify microbes based on their DNA or RNA.

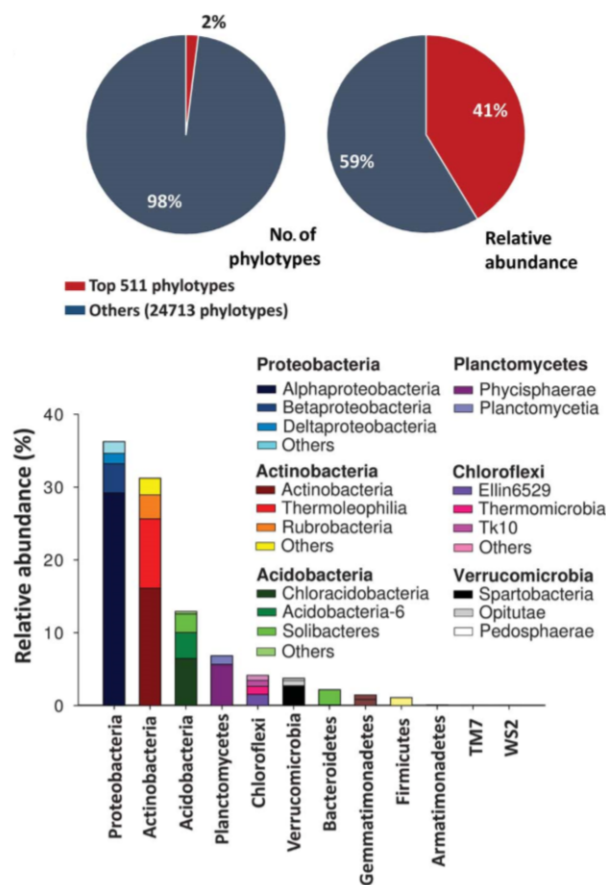


Figure 7: Left circle diagram shows the percentage of the most dominant soil bacterial phylotypes (Top 511 phylotypes). Right circle diagram shows the percentage that these dominant phylotypes represent in a soil bacterial community. Bar graph: Relative abundance of some dominant bacterial phylotypes (Delgado-Baquerizo et al., 2018).

Morphology bacteria

Bacteria can generally be classified in 3 types based on their morphology: round or spherical (cocci), rod-shaped (bacilli) or spiral (spirilli). However, many bacteria are pleomorphic meaning that they can have several shapes at once. When bacteria are motile, capable of moving, they have one or more flagella. A flagellum is a whip-like structure attached to one end, both ends or distributed around the cell body. Dependent on the adherence between the bacterial cells bacteria can form singles, pairs, chains or clusters (Orgiazzi et al., 2016). Bacteria grown in the laboratory average 0.5-1 μm in diameter and 1-2 μm in length (Pepper & Gentry, 2015). Orgiazzi et al. (2016) states that most bacteria are 0.2 μm in diameter and 2-8 μm in length.

2.2.2 Bacterial growth phases

Bacteria growth occurs in 4 phases (Fig. 8). After bacteria are fed with nutrients they do not immediately start to divide. For a period of time bacteria have to get accustomed to their new environment. This is called the Lag phase (1). After this phase the bacteria colony starts to grow exponentially. This is the exponential phase (2). After this growth period a stationary phase (3) occurs during which the amount of bacteria stabilizes. Finally a death phase (4) occurs in which a net loss of bacteria occurs. Some cells may still divide, but the majority of the cells die during this phase (Maier et al., 2009).

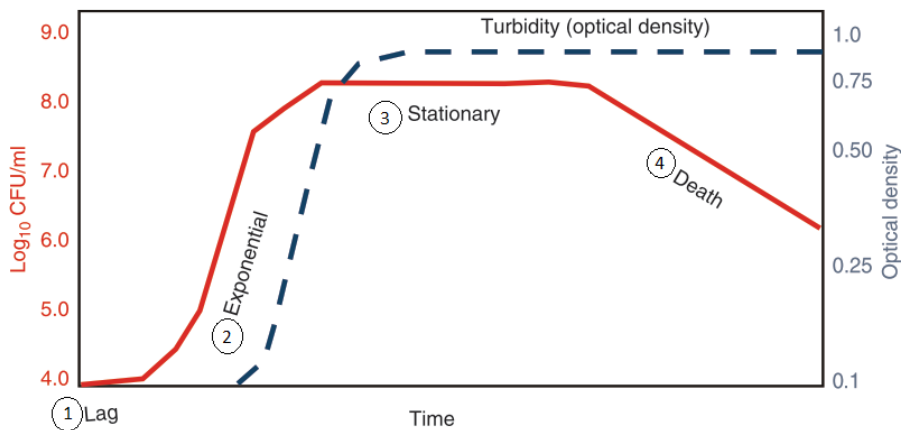


Figure 8: Bacterial growth curve (Maier et al., 2009).

Most knowledge about bacterial growth originates from laboratory experiments. These experiments are mostly conducted with pure cultures of bacteria under controlled conditions, while the natural subsurface environment may be very different and so may bacterial growth differ from experimental results. In laboratories not all factors affecting bacterial growth are taken into account. Therefore a cell division in the lab may take 10 minutes while it takes about 100 years in the natural environment due to heterogeneity in for example bacteria species and presence of nutrition.

2.2.3 Biomass formation

The rate of biomass formation has not been investigated so far, but an indication of it can be derived from the hydraulic conductivity measurements that has been done by several studies. Avnimelech & Nevo (1964) did percolation experiments with a cylindrical glass lysimeter with an internal diameter of 5 cm and a length of 45 cm. The height of the soil column was 30 cm. Bioclogging experiments that

make use of a column filled with sand generally last about a week to observe a remarkable amount of clogging (Leshchinsky & Ambauen, 2015)(Van Beek et al., 2007)(Liao et al., 2007). Whereas the few studies that used micromodels to simulate bioclogging lasted about 30 to 60 hours before clogging started (J.-W. Kim et al., 2010)(D.-S. Kim & Fogler, 2000).

Biomass is made up of bacterial cells (~10%) embedded in a matrix of hydrated exopolymeric substances (~90%) or exopolysaccharides (EPS). EPS is produced and secreted by the bacteria themselves, essentially to protect themselves from desiccation and other threats (e.g. pH conditions, unfavourable temperature) from their surroundings. The constituents of EPS depends on the type of bacteria, but are generally build up of polysaccharides, proteins, nucleic acids and lipids (Flemming & Wingender, 2010).

Biofilm formation (Fig. 9) occurs generally at a solid-liquid interface and (1) initiates with the attachment of cells at this interface. (2) Bacteria use organelles, as flagella and pili, to sense and attach reversibly to the surface. (3) The subsequent secretion of sticky EPS by the bacteria mediates an irreversible bonding between the cells and surface. (4) This ongoing accumulation of EPS leads to the formation of small microcolonies. Eventually a mature biofilm structure is formed. (5) At this stage some cells may detach from the biofilm, which may initiate biofilm formation elsewhere (Valiei, 2013)(Stoodley et al., 2002). When this process proceeds a bulk biomass forms at macroscopic level (Farah et al., 2016). Fig. 10 shows how this may look like below a microscope.

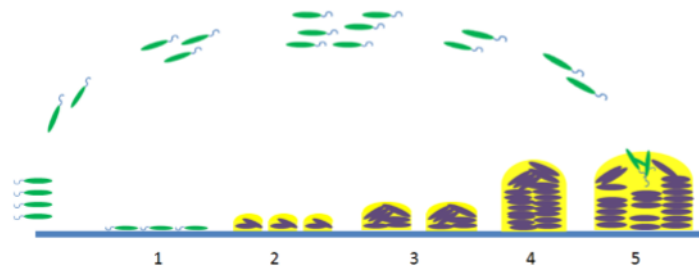


Figure 9: Biofilm formation stages. (1) Reversible cell attachment. (2) Irreversible attachment of bacteria to surface by EPS secretion. (3) Formation of biofilm microcolonies. (4) Mature biofilm structure. (5) Detachment of cells from biofilm (Valiei, 2013).

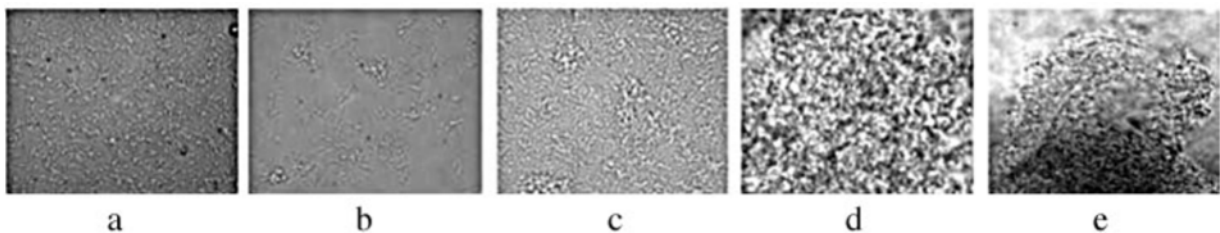


Figure 10: Photomicrographs of *P. aeruginosa* going through the five stages (a-e) of biomass development when growing under continuous conditions on a glass substratum (Stoodley et al., 2002).

This sequence of steps gives a general idea how biomass may grow, but it may also occur in another way. Vandevivere & Baveye (1992) shows with a column experiment that the distribution of biomass

across the pore space is dependent on several factors. They mainly observed biomass growth in aggregates throughout the pores and suggested this to be due to the glucose solution used as nutrition. Glucose has a low molecular weight and would therefore be rapidly metabolized by bacteria in the aqueous phase and subsequently growing biomass colonies in the pore space.

Whether a soil is suited for bioclogging depends on soil and water properties and is needed to know before the planning and execution of such projects.

A low C:N ratio caused rapid clogging, however the clog only lasted for a few days. A high C:N ratio on the other hand showed clogging after five days but was subsequently more sustainable. Also the degree of aggregation of dry sand was increased due to the high C:N ratio (Avnimelech & Nevo, 1964).

Almost all bacteria are able to secrete EPS when there is an excess of carbohydrates or other water soluble water sources of carbon over source of nitrogen (Ivanov & Chu, 2008)(Avnimelech & Nevo, 1964).

Intake of nutrition by bacteria can accelerate the production of EPS and thus the formation of biomass. Food-processing wastes or sub-products as a molasse with C:N > 20 are applicable for the production of bacterial water-insoluble polysaccharides (Ivanov & Chu, 2008).

A biofilm can occur in two basic forms: (1) as a capsule covalently bond to the bacterial cell surface, (2) loosely bond as a slime to the cell surface (Suresh Kumar et al., 2007).

Whereas Seifert & Engesgaard (2007) formulates the existence of three types of biomass distributions: (1) the biofilm approach with a uniformly distributed biomass, (2) a micro-colony approach with a non-uniform distribution and (3) a macroscopic approach, where the biomass is considered as a bulk average biomass with no further description of the geometry.

2.3 Bacterial identification methods

Fluorescence and Staining

Fluorescence is the emission of light coming from a molecule that has been excited by light with a certain (shorter) wavelength (Fig. 11). The incoming light gets absorbed by electrons bringing them in a higher energy state. Some of the absorbed energy will disappear as vibrational energy. If this energy loss is not enough to bring the electrons back to its initial ground state, it spontaneously emits photons with a higher wavelength. These photons are responsible for the fluorescent light coming from a specimen. The wavelength of the outgoing light is always longer than the wavelength of the absorbed light (Semwogerere & Weeks, 2005).

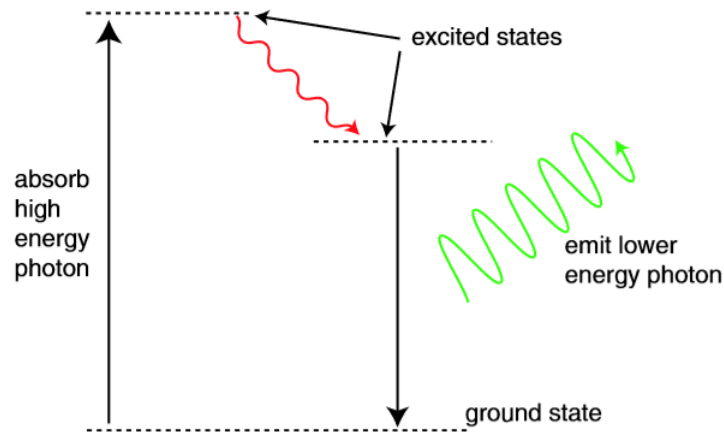


Figure 11: Fluorescence (Semwogerere and Weeks, 2005)

Many soil components (both minerals and organic substances) are autofluorescent and are thus capable to fluorescence by themselves after being excited by light with a certain wavelength (Li et al., 2004). Sediment particles can also have an intrinsic fluorescence property (Fuller et al., 2000). Autofluorescence from bacterial cells does not require labeling and virtually all of the bacterial species are autofluorescent (Bao et al., 2008). This phenomenon is called primary fluorescence. If molecules do not have this property they can be combined with a primary fluorescent molecule called a stain or fluorochrome to make them fluorescent. This is called secondary fluorescence (Li et al., 2004).

A variety of fluorophores can be used to stain cells in the laboratory (Fuller et al., 2000). Commonly used stains for bacterial cells are DAPI(4',6-diamidino-2-phenylindole dihydrochloride) and Acridine Orange (AO) (King & Parker, 1988) (see Fig. 12 for other commonly used stains). Both stains attach to the DNA or RNA of cells. DAPI gets excited with light of 360 nm (UV light) and emits light of 450 nm (blue light), while AO gets excited at light of 500 nm (cyan light) and emits light of 526 nm (green light) when attached to DNA (Kapuscinski, 1995). Fig. 13 and 14 show images of soil samples inoculated with *E. Coli* cells stained with Ethidium bromide or FITC.

Fluorochrome	Molecular weight	Excitation wavelength (nm)	Emission wavelength (nm)	Target	Color of stained cells
AO ^a	301.82	500 (DNA bound) 460 (RNA bound)	525 (DNA bound) 650 (RNA bound)	Nucleic acids	Green or red
CFW ^b	936.95	UV	NA	Polysaccharides	Violet
DAPI ^a	350.25	358	461	Double-stranded DNA	Violet
DTAF ^a	495.28	492	516	Protein, carbohydrates and polysaccharides	Yellow-green
Ethidium bromide ^a	394.31	518	605	Nucleic acids	Red
FITC ^a	389.38	494	519	Protein	Yellow-green
Mg-ANS ^c	311.00	385	485	Protein and membrane	Blue
Thiazine red R ^{b, c}	599.58	UV	NA	NA	Red
Thiazol yellow G ^{b, d}	695.73	402	NA	NA	Yellow to greenish

^a Molecular probes (2003)

^b Altemüller and van Vliet-Lanoe (1990)

^c Florida State University (2003)

^d Lillie (1977)

Figure 12: Commonly used stains for soil microbiological studies and their properties (Li et al., 2004).

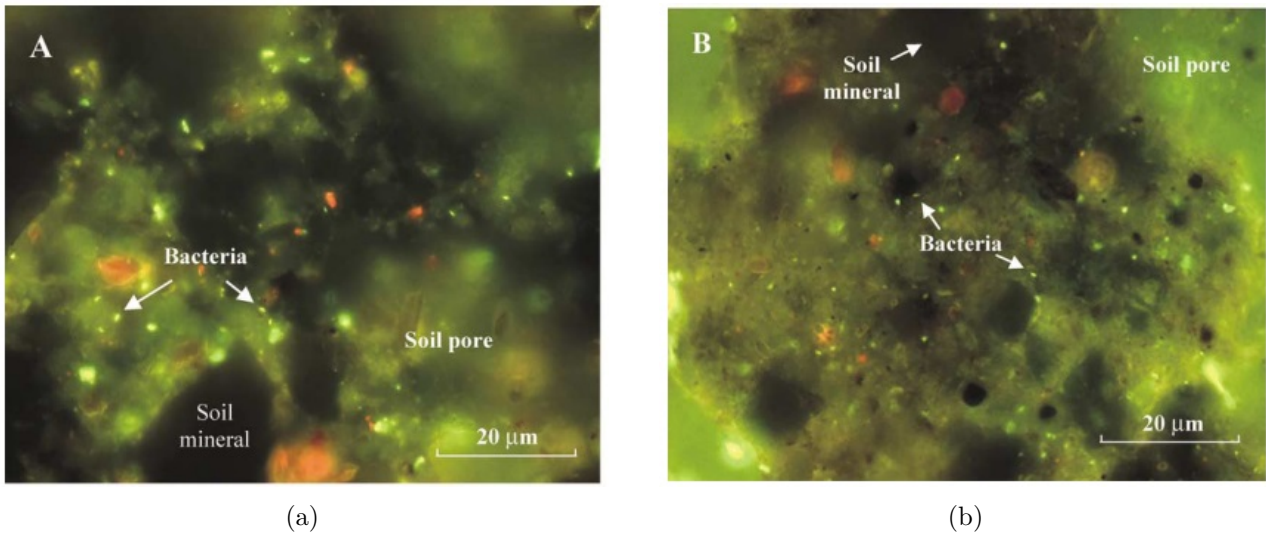
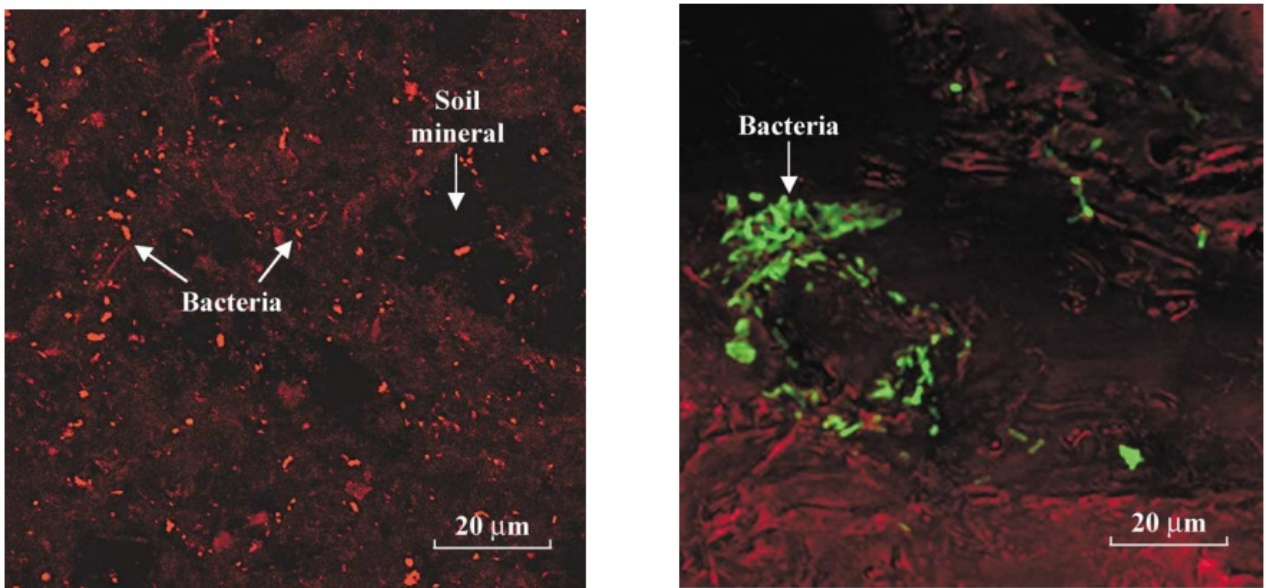


Figure 13: bacteria stained with ethidium bromide in a silt loam soil inoculated with *E. coli* (Li et al., 2003).



(a) Ethidium bromide-stained silt loam soil that had been inoculated with *E. coli*. Excitation wavelength was 488 nm.

(b) FITC-stained sandy soil inoculated with *E. coli*. Excitation wavelength was 488 nm. Green=bacteria, Red=sand.

Figure 14: Projection image of 25 confocal serial sections (taken at 0.4 mm increments) (Li et al., 2003).

OD600

The OD600 is the optical density of a sample at 600 nm. Light with this wavelength is transmitted by bacteria and other organic material. Measuring this quantity through time with a spectrophotometer gives an estimation of the concentration of bacteria in the sample and the rate of growth (J.-W. Kim et al., 2010). A further description of this method applied for this study is given in Section 3.1.

2.4 Clogging factor

The degree of clogging over a certain path can be quantified by the clogging factor². This factor is a ratio between the hydraulic conductivity at some time t during the experiment and the initial hydraulic conductivity over a certain path. Darcy's law is used to determine the clogging factor:

$$Q = -k \frac{\phi A}{\Delta h}$$

where Q (m^3/s) represents the volumetric flow rate, $\Delta\phi(m)$ is the hydraulic head difference between two specified locations along the flow path, A (m^2) is the cross-sectional area the fluid is flowing through.

By rewriting this equation for the hydraulic conductivity k , the initial hydraulic conductivity k_i at $t=0$ and the hydraulic conductivity $k(t)$ at some time t can be determined:

$$k_i = -\frac{Q\Delta h_i}{\phi A}$$

$$k(t) = -\frac{Q\Delta h(t)}{\phi A}$$

The clogging factor follows from dividing k_i by $k(t)$:

$$clogging\ factor = \frac{k(t)}{k_i}$$

²Document received from Deltares

3 Methods and materials

This Section explains the methods applied for this study and a description of the laboratory equipment used. Besides, the experiments are explained and the origin and composition of the solutions used are given.

3.1 Spectrophotometry (OD600)

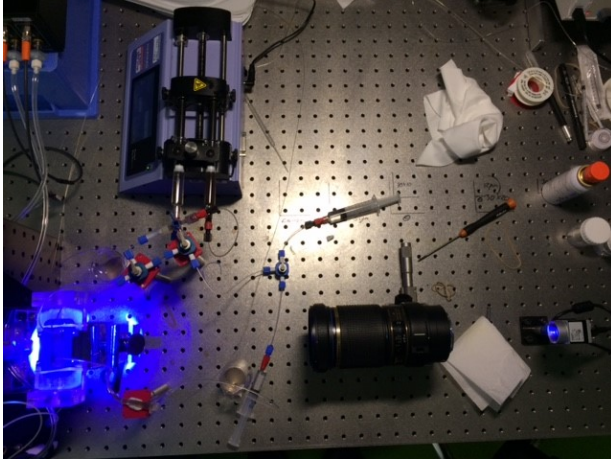
A spectrophotometer is an instrument that measures the intensity of a light beam that reaches a detector after it has travelled through a sample. The ratio between the intensity of the incoming and outgoing light determines the absorbance or optical density of the sample. The value of absorbance is representative for the presence of a certain substance in the sample.

In this case it measures the optical density for light with a wavelength of 600 nm to obtain. The light with this wavelength does not kill bacterial cells. Therefore this method is generally preferable above UV spectroscopy that is also applied for bacterial analysis but might kill the bacteria.

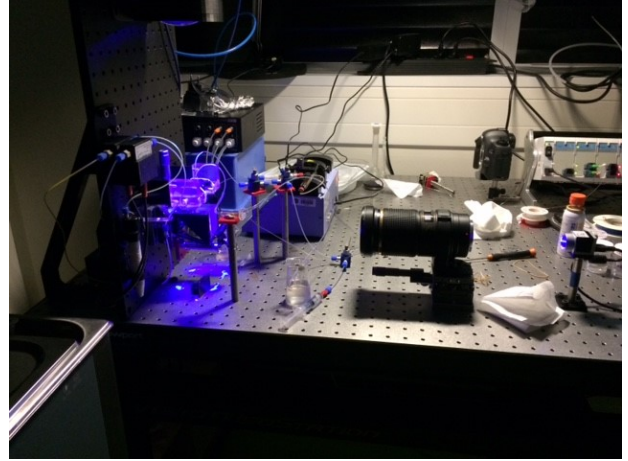
3.2 Open microscope set-up

The open-microscope set-up (Fig. 15) was positioned on a table and consisted of a syringe pump including two syringes, one filled with groundwater the other with diluted Nutrolase. The syringe pump can manually be installed at a specific flow rate. The content of the syringes are either sucked out of the syringe or injected from it towards the micromodel via plastic tubes. Plastic tubes are connected to the syringes and used as flow pathways towards a micromodel. The fluids also leave the micromodel flow via a plastic tube into a measuring cup. During the experiment images are taken of the porous medium in the micromodel with a digital photo camera, which was fastened to the table. Besides, a pressure transducer was installed to the system to measure the pressure before the inlet and after the outlet of the micromodel. For the first experiment the pressure transducer was nulled with the atmospheric pressure (≈ 100 kPa) to have a reference pressure level of 0 kPa. For the second experiment this was forgotten to do, causing these values to have a reference level of approximately 100 kPa. However, as the pressure difference between the inlet and the outlet is of interest this does not influence the hydraulic gradient across the micromodel.

Before injecting the solutions, CO_2 is injected to replace the oxygen-bearing air in the pores. As the solubility of CO_2 is higher than the solubility of oxygen it prevents gas to become entrapped in the pores. Therefore full saturation of the porous medium with liquids can be achieved easier. This method was applied for the first micromodel experiment. As this did not completely worked out ethanol was injected instead of CO_2 for the second micromodel experiment to get saturated initial conditions. Ethanol also has a high water solubility and makes it more favourable to achieve saturation conditions as no air was present in the pore space at the beginning of the second experiment.



(a) Top view.



(b) Side view.

Figure 15: Open microscope set-up.

The experiments were performed in a dark room, to limit the influence of light on bacterial growth. Especially UV radiation is lethal for microorganisms as bacteria (Hockberger, 2000). An exponentially increasing radiation dose is required for killing a certain fraction of *E. coli* cells when raising the wavelength of light from the visible light spectrum. Blue light is on the left side of the visible light spectrum with a relatively short wavelength. Thus this light is relatively less harmful to at least *E. Coli* cells (Vermeulen et al., 2008) and also other bacteria (Kamel et al., 2016). Besides the higher the radiation dosage for any light colour, the higher its effect on the viability of the bacteria (Vermeulen et al., 2008). Therefore, it was chosen to dim the light for the second micromodel experiment.

Micromodel

The micromodel (Fig. 16) is made of PDMS (Polydimethylsiloxane), an optically transparent, artificial, flexible and hydrophobic material. This material is often used for e.g. biological and fluid flow experiments (Abolmaaty & Meyer, 2017)(Roh et al., 2016). Although an disadvantage of PDMS is that the hydrophobicity may change with time and space (Karadimitriou & Hassanizadeh, 2012). The micromodel contains two inlet channels and one outlet channel. One inlet is used for the injection of groundwater, the other for the injection of Nutrolase. The outlet is kept open all the time. Between the inlets and the outlet, a very thin layer of an artificial porous medium is located. The porous medium is 1 cm long and 1 cm wide. The depth of the porous medium is 69 μm . The artificial grains of the porous medium have different sizes and are randomly distributed to mimic a real porous medium as close as possible. Different porosity levels are used for this study to observe its effect on it.

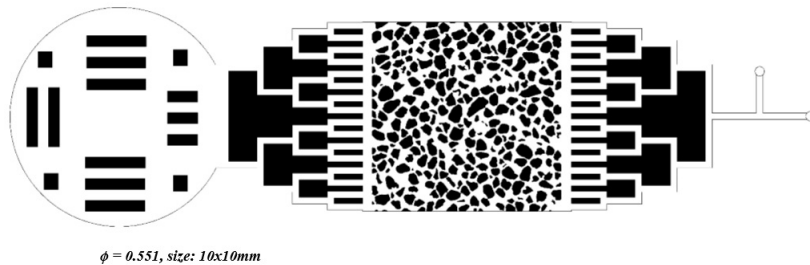


Figure 16: Digital representation of a PDMS micromodel.

3.2.1 Confocal Laser Scanning Microscope (CLSM)

A Confocal Laser Scanning Microscope (CLSM) is a microscope that uses laser to make high-resolution images of a (specific part of a) specimen. While an optical microscope enlightens an entire specimen a CSLM illuminates only a specific part of a specimen due to two pinhole apertures. These pinholes block any out-of-focus laser light and light coming from the surroundings. This increases the resolution of the created images of the specimen and focuses the light on a specific plane of the specimen. A plane that could not be sectioned physically. Due to the ability of depth selection one can create high-resolution 2D and 3D images.

How does a CLSM work?

A light source emits a laser beam with a specific wavelength (Fig. 17). When the focused light has passed the pinhole aperture and excitation filter the light is reflected by a dichroic mirror towards the specimen. This dichroic mirror reflects light shorter than a specific wavelength and passes light above this specified wavelength. Thereafter, the reflected light is converged by an objective lens radiating the light on the point of the specimen that will be excited. The excited point will back radiate fluorescent light in the direction of the objective lens and dichroic mirror. Also out-of-focus light that comes from the sample is radiated. Both in-focus and out-of-focus light pass the objective and the dichroic mirror towards another pinhole aperture that blocks all out-of-focus light. Hereafter only in-focus light is received by the photomultiplier detector that eventually creates a high resolution image (Semwogerere & Weeks, 2005).

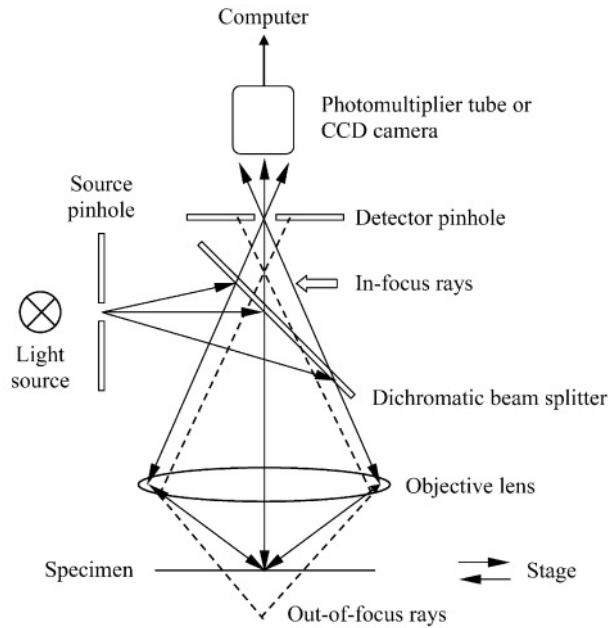


Figure 17: Configuration of a confocal laser scanning microscope (Li et al., 2004).

As the bacteria in the groundwater are not fluorescent by itself, specific fluorescent particles need to be added to be able to make the bacteria and produced biomass visible through the confocal microscope. To know which fluorescent particles attach to the bacteria, the size of the bacteria needs to be determined.

3.3 Experiments

3.3.1 OD600

Before use of the spectrophotometer, the vials in which the solutions will be prepared are rinsed with distilled water and the autoclaved at 121°C for 30 minutes. This way the vials are as sterile as possible and causes the initial conditions of the vials to be more or less similar. When the vials are sterile, they are filled with groundwater using a micropipet.

First of all, a cuvette filled with demineralized water was measured with the spectrophotometer as a measure of reference. After measuring this value, the spectrophotometer was calibrated for this value by pressing the Auto zero button of the apparatus. Subsequently, three different groundwater samples were taken from the stock groundwater and measured at different time steps.

Before taking groundwater out of the beaker glass for the first time, it is shaken to have a heterogeneous distribution of bacterial cells in the groundwater as far as possible. The optical density of this sample was hereafter measured at $t=0$ minutes and $t=15$ minutes.

The second sample was taken from the beaker when the cells were already a bit settled at the bottom of the beaker. This is done to see whether the optical density also drops when the bacteria and/or particles are settling. The measurements for this sample were taken after 0, 5, 10 and 15 minutes.

For the third sample, the groundwater was even further settled. This sample could support the existence of bacteria in the groundwater even more. This sample was measured once at $t=0$ minutes.

3.3.2 Micromodel experiments (Open microscope)

Table 1 shows the specifications used for the micromodel experiments imaged with the open microscope set-up. A detailed description of the experiments is followed up in this Section.

	Saturation by	Suction/injection	Q (ml/hr)	Light	ϕ (-)	Image frequency	Total time (hr)
Exp. 1	CO_2	Suction	0.05	Blue	0.55	1/10 min	65
Exp. 2	Ethanol	Injection	0.05	Blue (dimmed)	0.50	1/30 s	17

Table 1: Experiment specifications

Experiment 1

The first experiment was a first try out with the open-microscope set-up. The goal for this experiment is to simulate bioclogging in a micromodel by injecting groundwater and Nutrolase through the micromodel.

To start with a saturated micromodel with groundwater, CO_2 was injected into the micromodel followed up by the injection of groundwater. As CO_2 is better dissolvable than air in groundwater. Unfortunately, still some air got stuck in a few pores at the edge of the micromodel.

Next, groundwater and Nutrolase were sucked into the micromodel at a volumetric flow velocity of 0.05 ml/hr. This flow rate is presentative for a fluid flow through a sandy porous medium (J.-W. Kim

et al., 2010). Nutrolase was diluted 4 times with tap water. This value is a flow velocity representative for a sandy porous medium. The micromodel, with a porosity of 0.55, was enlightened with blue light. Every 10 minutes a photo was made of the micromodel and every 5 seconds a measurement of the pressure across the micromodel was made. The total time of this experiment was 65 hours. This was an estimated time to be able to have sufficient time for the biomass to grow and because the experiment was started on a Friday. So the experiment could continue during the weekend.

Experiment 2

A similar experiment as the first experiment has been executed a second time but with a few configurations. Instead of suction, injection of the fluids was applied. This would hopefully work better for the experiment. Also ethanol instead of CO_2 has been used to have better initial saturation conditions than the previous experiment. Ethanol is just as CO_2 dissolvable in water.

The same dilution ratio and flow rate were used. Although the porosity of the micromodel was 0.55 and the blue light was dimmed as this could affect the growth of the bacteria. The frame rate was 1 photo per 30 s and the total experiment lasted 17 hours. The reason for the higher frame rate is that it would help with getting a better view on what happens in the micromodel and where undesired air possibly could come from. Because of this frame rate the amount of images also increases. Therefore, the time of this experiment is a bit shortened in comparison with the first experiment.

3.3.3 CLSM experiments

Before conducting a dynamic micromodel experiment with the confocal microscope, a few static observations of the fluids involved during BioSealing are done. These static observations are useful to know how the fluids look like below the confocal microscope and to recognize the different components of the fluids. The confocal microscope is connected to a computer so it can be used to observe the sample of interest and to make images of it (see Appendix A.2). The software used for the observations is NIS Elements.

At first, the fluids are observed separately. A droplet of groundwater is put on a glass slide covered by a cover glass and observed with the confocal microscope. Also Nutrolase is observed separately. These samples are observed with different filters as certain particles of the fluids are more susceptible to a specific wavelength than another. A few images have been taken of a sample with a fluorescent added to it which could attach to the constituents of the fluids and potentially brighten the bacteria in the groundwater. By using the right filter on the confocal microscope, the bacteria could be visualized. The fluorescent used is called Fluoresbrite (YG) microspheres that looks like a green fluid suspension. These microspheres have carboxylate groups on their surfaces that can be activated for the covalent coupling of proteins. However, the microspheres may also adsorb to other particles when using it in excess and soil particles may also cause background fluorescence when excited with light of a certain wavelength (Li et al., 2004).

The maximum excitation wavelength of Fluoresbrite (YG) is 441 nm and its maximum emission wavelength is 488 nm. The radius of the fluorescent particles is either $0.5 \mu\text{m}$ or $0.75 \mu\text{m}$ ³. This fluorescent is extensively used for phagocytosis studies, flow cytometry and diagnostic assays. These also involve staining of bacteria (Sakamoto et al., 2005).

³both are present in the laboratory where I worked, but I did not check which one I used

3.4 Solutions

3.4.1 Groundwater

The groundwater used for the experiments originates from an uncontaminated agricultural area with a peat-like soil in the Province of Groningen (The Netherlands). It contains many types of (harmless) bacteria. The bottle with groundwater (200 ml), I received from Deltares⁴, contains more bacteria than there are people on Earth. By adding nutrition to this bacterial population the amount of bacteria will even be multiplied by several billions.

The depth of extraction of the groundwater was about 3m, which was 1,5 m below the groundwater level. This means that both aerobic and anaerobic bacteria are present in the water. The pH of the water is 5.5, which is relatively low for groundwater. Before usage for this study the water has been preserved in a bottle containing nitrogen gas in the headspace to prevent organic material in the water from rotting.



(a) Extracting groundwater.



(b) Groundwater level measuring well.

Figure 18: Manual groundwater extraction, Utrecht Science Park.

After all the aforementioned groundwater had been used and was not at stock anymore, new groundwater has been pumped from a groundwater level measuring point with the help of a groundwater specialist of RPS as this company owns this well and could give me the equipment needed to pump up groundwater (Fig. 18a and b). The groundwater is extracted from a depth of about 3 meter, just below the groundwater table. The composition and presence of microorganisms in this groundwater was not known.

Eventually this groundwater has not been used anymore for any of the experiments discussed in this report. It was planned to use this groundwater for further experiments with the confocal microscope, but unfortunately this was not possible anymore due to the closing of the laboratory as a consequence of the ongoing Corona pandemic.

⁴private communication

3.4.2 Nutrolase

To increase the rate of the biomass production in the pores a nutrient solution is added to the microfluidic system. Previous research on BioSealing by Deltares (2003) with Nutrolase showed that this is an effective nutrient solution for the bacteria. Nutrolase is a protamylasse, a waste product of processed potatoes containing a blend of organic acids, sugars, proteins, amino acids and various salts (see Table 2). Its variety in constituents makes it applicable for various bacteria. The solution contains a small amount of solids that may cause plugging, therefore the solution is sieved prior to use. For this study the solution is diluted four times to prevent the viscous solution from clogging the system.

This substance is mainly applied in soil remediation cases to stimulate the growth of certain micro-organisms. It also lowers the redox potential of the soil creating optimal circumstances for dehalogenation, i.e. the degradation of the harmful carbohydrates into less harmful products by the influence of the micro-organisms.

Component	Concentration (mg/l)
Phosphor	6400
Sulfur	12000
Nitrogen	32000
Crude protein	199000
Amino acids	147000
Sugars	
Fructose	31000
Glucose	31000
Sacharose	61000
Reduced sugars	45000
Organic acids	
Acetic acid	3500
Lactic acid	11000
Oxalic acid	5200
Malic acid	31000
Citric acid	62000
Cations	
Potassium	80000
Magnesium	4100
Calcium	580
Sodium	580
Ammonium	3500
Anions	
Chloride	4100
Nitrate	1740
Sulphate	18000
Phosphate	20300

Table 2: Chemical composition of Nutrolase.

4 Results

4.1 OD600

The first sample that was measured was a cuvette filled with demineralized water to have a reference level of the optical density of plane water and the cuvette as this also absorbs some of the incoming light. The optical density of this sample was 0.0549. This value is taken into account in the measured values for the 3 groundwater samples. So the values shown in Table 3 are representative for the particles present in the groundwater (GW).

	t=0 min	t=5 min	t=10 min	t=15 min	t=25 min
GW (shaken, not stirred)	0.315	-	-	-	0.021
GW (almost settled)	0.0191	0.0179	0.0179	0.0179	-
GW (further settled)	0.0062	-	-	-	-

Table 3: Optical density measurements (600 nm) of groundwater (GW).

The first groundwater sample had an optical density of 0.315 at the beginning. After 35 minutes this value is decreased to 0.021. The second sample taken 30 minutes after the groundwater in the bottle was shaken measures an initial value of 0.0191 and then decreases to 0.0179 in the first 5 minutes. During the following 10 minutes the optical density stays the same. A last sample was taken and measured once. This optical density was 0.0062.

A sequence of measurements has been done later as well. Fig. 19 shows the progression of the optical density of a groundwater sample for 15 minutes. The general trend of the graph shows that the optical density decreases irregularly from 0.09 to 0.05 during these 15 minutes. Looking closer at the graph shows that a significant decrease starts in the first 3 minutes. The value drops to approximately 0.065 in this time. Hereafter the optical density stays more or less around this value the following 10 minutes. Between t=8 minutes and t=10 minutes, the optical density rises slightly above 0.07 ending with a sharper decrease to 0.05 during the last 3 minutes of the experiment.

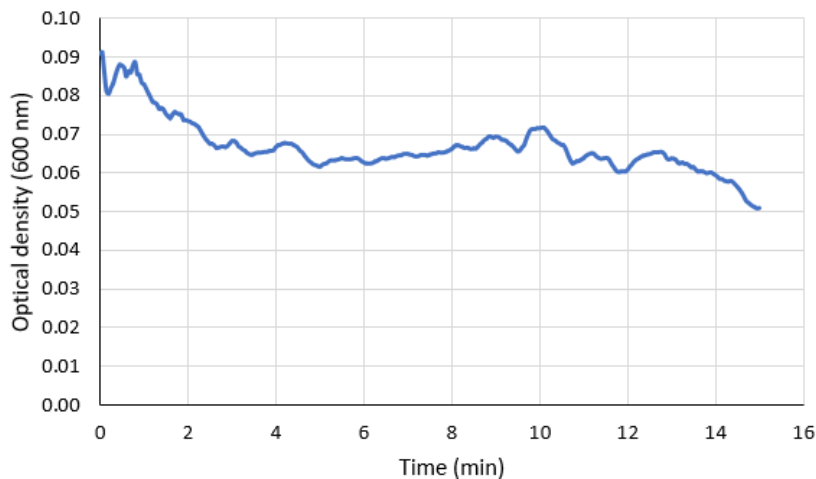


Figure 19: Optical density (600 nm) of groundwater through time.

Besides to check whether the optical density depends linearly on the concentration of particles in the groundwater, a regular groundwater sample has been taken and measured and compared with a diluted groundwater sample. The groundwater sample was diluted 1:1 with demi-water. The same groundwater of the regular sample was taken for the diluted sample. Prior to these measurements, the spectrophotometer was calibrated by measuring the OD of demi-water. This value was 0.0534. The groundwater sample measured 0.016 and the diluted sample 0.0067.

4.2 Micromodel experiments (open microscope)

4.2.1 Experiment 1

The images in Appendix A.1 show the most significant occurrences during the entire experiment.

t=0 hr: As mentioned in the Methods Section this experiment initiates with some air stuck in the pores along the edge of the micromodel, but the other pore space is filled with groundwater (Fig. 22a). Also some black spots and strings can be observed throughout the pore space, but also on or inside the PDMS grains. These spots stay there during the entire experiment and seem to be irregularities in the micromodel itself. The flow direction of the injected fluids is from left to right.

t=2.5 hr: While the groundwater flows through the micromodel more air is coming into the micromodel via the inlet and spreads around the majority of the pore space (Fig. 22b). The air resides in both the small as well as the large pores. The interfaces between the groundwater and the air phase is predominantly convex for the air phase and concave for groundwater. Also a few more black spots are visible in the pore space along some grains. They typically seem to attach to the grains while inside the air phase.

t=14.5 hr: With time, the air keeps moving around the pore space and even flows partly against the ongoing flow direction towards the inlet channels. Later the black spots seem to grow and spread around heterogeneously in more pore spaces. These accumulations are more coarsely grained and seem to be built up of smaller sized particles connected as bridges between grains (Fig. 22c). The boundaries of these accumulations seem to be concave. Thin but pitch dark spots are also visible along grain boundaries.

t=25 hr: The accumulated particles become more densely packed and darker coloured (Fig. 22d). They are also found at different places than at t=14.5 hr. At some places the accumulations are black.

Every now and then a light grey pulse of fluid flow is entering the pore space and finds a way through the pore space filled with air.

t=31.7 hr: The boundaries of several air bubbles start to get thick and black mostly throughout the upper part of the micromodel (Fig. 22e). Meanwhile about 90 percent of the pore space is filled with air containing the grey material, but in smaller extent.

t=65 hr: At the end of the experiment most of the pore space was filled with air that was greyish on the interior and black at some boundaries (Fig. 22f).

Pressure gradient and clogging factor

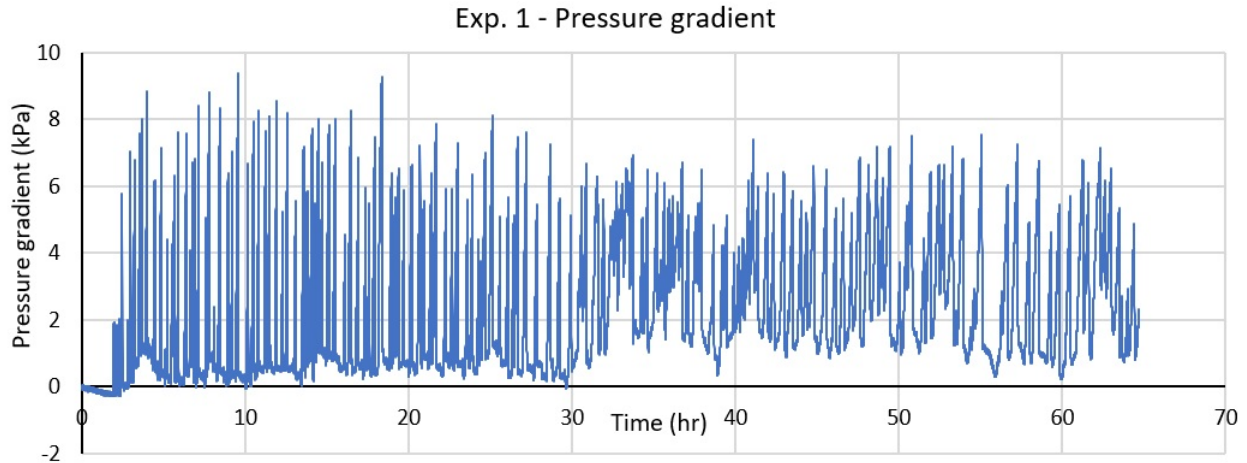


Figure 20: Pressure gradient development across micromodel (exp. 1).

The pressure gradient as shown in Fig. 20 shows a zigzag pattern of pressure gradient values fluctuating between almost 0 kPa and 9.5 kPa at its maximum. But before the pressure gradient rises for the first time it slightly decreases the first 2 hours from 0 kPa to -0.12 kPa. After 30 hours the minimum pressure gradients are a bit higher (≈ 1.0 kPa) whereas the highest pressure gradients are peaking at a lower value (≈ 6.5 kPa).

Due to the measured initial pressure gradient of almost zero and the presence of air at the beginning of the experiment a reliable value for the hydraulic conductivity without any clogging could not be calculated and therefore the clogging factor could not be calculated.

4.2.2 Experiment 2

Due to the injection of the fluids into the micromodel instead of suction, the flow direction during this experiment is from right to left as also shown in the images of Fig. 23a-h.

t=0 hr: The micromodel was fully saturated with groundwater at the beginning of the experiment (Fig. 23a).

t=2.25 hr: With time the incoming fluid becomes gradually greyer (Fig. 23b).

t=2.5 hr: With pulses some black particles are flowing into the micromodel (Fig. 23c).

t=4.4 hr: Some of these particles travel through the pores and eventually leave the micromodel through the outlet channels, while also with time progressively more particles get stuck along or between the grains (Fig. 23d).

t=4.52 hr: An even larger and denser pulse of a dark mass suspended in the fluid flow enters the micromodel after about 4.5 hours (Fig. 23e). It leaves behind tracks of the dark material in the pore space.

t=4.86 hr: After nearly 5 hours a large pulse of air is suddenly coming into the micromodel from the inlet channels (Fig. 23f)

t=4.925 hr: The air spreads around the pore space of the micromodel (Fig. 23g).

Little of the dark material that was occupying the pore space is left in the micromodel as it is pushed away towards the outlet channels. The air is also present in (all) the inlet and outlet channels and has thick black boundaries. At some time a light grey fluid flow pushes some air away from one of the inlet channels and finds a way through the pore space towards the outlet. The colour of this fluid is lighter than the fluid suspension that is still partly present in the pore space next to the air phase.

The following hours the air moves around the pore space and also sometimes leaves the micromodel.

t=16.3 hr: At the end of the experiment the pore space is filled with air bubbles with thick boundaries and the grey material (Fig. 23h).

Pressure gradient and clogging factor

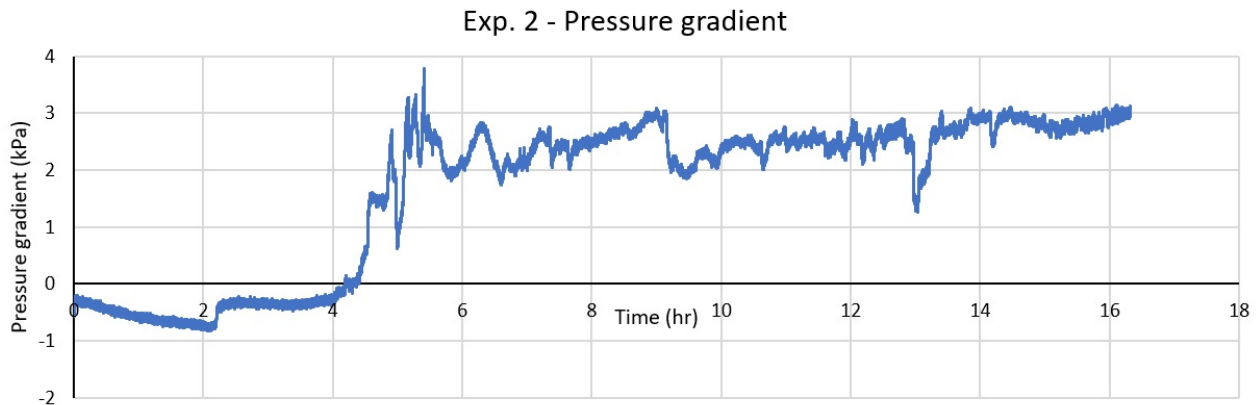


Figure 21: Pressure gradient development across micromodel (exp. 2).

The pressure gradient across the micromodel for this experiment initiates with values below 0 kPa the first 4 hours (Fig. 21). After this period a sudden rise to a peak value of about 3.8 kPa is visible. Subsequently the pressure gradient stabilizes more or less and fluctuates around a mean value of about 2.5 kPa until the end of the experiment. After about 9 hours and 11 hours sudden pressure gradient drops are seen. Although it seems that the gradient keeps fluctuating around 2.5 kPa, it looks like that at the end of the experiment the pressure gradient is continuously increasing.

Also for this experiment the pressure gradient values at the start of the experiment are unreliable to use for the calculation of the clogging factor.

4.3 CLSM images

The images made with the confocal laser scanning microscope described in this Section can be found in Appendix A.2. The red scale bar at the right bottom of Fig. 26 and 27 shows the length of 100 μm .

Fig. 24a and b show the same droplet of groundwater but observed with 561 nm-filter (Fig. 24b) or without filter (Fig. 24a). In Fig. 24a the boundaries of the droplet can be observed in the topleft and bottomleft corner. Inside the droplet many round particles can be observed with varying sizes. These particles are approximately 10 μm in radius, but some are even as small as a few μm in radius. When using a filter with a 561 nm wavelength, three relatively large particles enlighten in red colour next to many small particles mostly visible in the left-down corner of the image.

Nutrolase on the other hand, also consists of particles of different sizes, but the size range is more variable. These particles can be more clearly seen when a sample of diluted Nutrolase is observed (Fig. 25a), while a pure sample of Nutrolase shows a big mush of particles (Fig. 26a). The smallest particle seems to be 1 μm , while the largest is approximately 40 μm . A large accumulation of these particles can clearly be seen in a sample of diluted Nutrolase in groundwater (Fig. 26b). An image of diluted Nutrolase with demi-water with a 561 nm-filter shows that all particles reflect the colour transmitted by this filter (Fig. 25b).

Fig. 27 shows images of different samples with Fluoresbrite added to it and observed at different wavelengths. The normal view of the first groundwater sample (Fig. 27a-left bottom) shows a few irregularly shaped particles inside the lightgrey matrix (black and grey area below this is outside the sample). The 405 nm-filter does not show any features, but the particles in the normal image are visible in the 488 nm-filter. It even shows many very tiny particles in the matrix of the sample. A sample of groundwater with Nutrolase and added Fluoresbrite shows many fluorescent particles for both wavelengths (405 and 488 nm) (Fig. 27b,c). The particles are barely distinguishable in the normal image, but are more clearly visible in the filtered images which both show the same fluorescent particles.

5 Discussion

5.1 OD600

First of all, from the decline of the optical density of the groundwater samples with time can be derived that this can be explained by the settlement of particles in the groundwater. Due to the settling less particles interfere with the incoming light of 600 nm wavelength resulting in a lower optical density value. At the beginning of the measurements the optical density decreases quickly as the largest and heaviest particles settle. These particles obstruct the majority of the incoming light. Later during the experiment smaller particles settle causing minor decrease in optical density.

Whether the particles are bacteria is difficult to determine from these results. The wavelength of the light (600 nm) should be favourable for the determination of the biomass in the groundwater. The colour of the groundwater is slightly yellow with a wavelength close to 600 nm. This might influence the measured data. Also organic material other than bacteria might scatter the incoming light of 600 nm causing the measured value to increase.

5.2 Micromodel experiments (Open microscope)

5.2.1 Experiment 1

The initial expansion of the air present at the beginning of the experiment is possibly due to air that enters the micromodel through pores of the material of the micromodel itself from the outside. Another possibility is that there is a leakage in the tube network before the micromodel where air may enter the system. As mentioned before the BioSealing process also involves a fermentation reaction of the Nutrolase solution due to the bacteria. An end product of this reaction is a smelly gas. Therefore the air in the micromodel might be this gas, although it might have been smelled in the experiment room at the end of the experiment which was not the case. To verify whether this is truly the fermentation gas, it could be captured and smelled for example as a follow-up experiment. A third option is that the air comes from the injected water that is saturated with air and may be released and grow due to a change in temperature or pressure in the system.

Which option is most reliable is left aside, but at least it can be supposed that it most probably does not come from the BioSealing reaction itself. Besides, The air is already present in the micromodel before the start of the experiment. A PhD-student of the Environmental Hydrogeology Group (UU), who also executed micromodel experiments with this set-up, had similar problems with air being trapped in the pore space of a micromodel and also could not find the cause for this problem.

The dark or grey material that accumulates inside the air is difficult to identify. It might be particles of Nutrolase or biomass. Bacteria are generally not larger than 10 μm , so are not separately visible on the images, but it could be accumulation of bacteria with EPS, so-called biomass. Typically they attach to the grains. On the other hand it is quite debatable whether the dark particles are bacteria or biomass. During an growth experiment of the bacteria by J.-W. Kim et al. (2010) they observed a lag phase of the bacteria growth that lasted about 10 hours and the peak value of bacteria concentration was reached after 20 hours. This does not resemble the time interval for appearance of the black particles for this experiment.

The initial small but remarkable decrease in hydraulic gradient across the micromodel, reaching values below 0 can be explained due to fluctuations in the sensors of the pressure transducers. Especially in case of no flow the pressure transducer is not able to measure a constant pressure value.

These no flow conditions were possibly present due to the delay of incoming fluids. As suction was applied for this experiment the syringes were not tightly attached to the syringe pump. This means that there is some space causing the syringe pump not pulling immediately on the syringe. This leads on its way on a period of no flow at the beginning of the experiment. As a relatively low flow velocity was applied with the syringe pump, this delay in fluid flow can take a few hours. Meanwhile air is able to enter the system through the outside of the micromodel.

J.-W. Kim et al. (2010) concluded that a low flow velocity (1.25 mm/min) resulted in a slow but eventually higher clogging degree compared to a high flow velocity (7.5 mm/min). The decrease of the hydraulic conductivity began after about 30 hours for the low flow velocity experiments. The flow velocity used during my study (2.2 mm/min) comes closer to the lowest flow velocity used by J.-W. Kim et al. (2010) than the highest flow velocity. Therefore it would have expected that the clogging during my experiments would also begin after about more than one day. But the graph of Figure 20 shows that a significant clogging event already starts after about 2 to 3 hours. Although it needs to be mentioned that this clogging, and clogging for the entire experiment, is due to the air accumulation in the pore space instead of the biomass formation. This causes the relatively early measured increase in pressure gradient across the micromodel. Whereas the experiments of J.-W. Kim et al. (2010) did not involve clogging due to air accumulation but only by biomass.

As above-mentioned the majority of the clogging is due to the air accumulation. Also due to the dynamic behaviour of the air throughout the pores the pressure gradient across the micromodel fluctuates significantly between a high and low gradient. Most of the time the air is distributed in such a way that the incoming fluid is barely able to reach the outlet of the micromodel, but at recurring moments a free flow path appears that connects the inlet with the outlet. This might lead to a sudden decrease in the hydraulic gradient. Although still the air covers most of the pore space, it would not be expected that the hydraulic gradient would drop to almost zero as shown in Fig. 20. This would mean that there is almost no resistance for the incoming fluid flow.

The growing mass inside the air phase has not probably a large impact on the hydraulic gradient as it exists inside the air.

The sudden change in the pressure gradient pattern at 30 hours is relatable to an occurrence in the micromodel at this time. The grey mass present inside the air spreads across the boundaries of the air bubbles and between 30 to 40 hours seems to dissolve into the ongoing fluid flow as this is getting a bit greyer. A colour that is quite similar to the colour of the air. Besides looking at the pressure increases it is remarkable that it mostly only happens when the pore space is in at least for 80% occupied with air. When the fraction of pore space is filled with air decreases below this threshold the pressure gradient decreases significantly to 1 or almost 0 kPa.

As mentioned before, it was not able to calculate the clogging factor for this experiment, but it can be derived from the episodic increases of the hydraulic gradient throughout the experiment that the pore space was clogged extensively.

Although this experiment seems to have a major problem with air clogging, there is also a positive side on this experiment. The extent of the clogging by the biomass, as far as it can be concluded that the dark matter is biomass, is not excessively high and not blocking complete pathways from the inlet to the outlet of the micromodel. Especially on this scale it is not favourable to have significant clogging due to biomass growth taking into account the larger scale application of this method in the field. If the micromodel would have been clogged almost completely by the biomass, clogging in the

field would probably also occur at a low-depth in the soil. The biomass would not reach the cracks in the bedrock below the soil, which is the actual target.

The presence of an air phase in the pore space affects the fluid dynamics, but so does the hydrophobic property of the material of the PDMS micromodel. Nonetheless, the groundwater seems to be the wetting phase when looking at the curvature of the interface between groundwater and air. The boundary of the groundwater is concave and the boundary of air convex. So the groundwater is the wetting phase.

As the pore space during the entire experiment is filled with air and water, multiphase flow and thus relative permeability is relevant for the effective flow through the porous medium. As the saturation of air rises significantly from the beginning of the experiment, the relative permeability of water decreases significantly as a consequence. So as the ongoing drainage occurs, initially the capillary pressure increases slowly. Although with increasing air saturation towards approximately 80%, the capillary pressure increases fast as the main drainage curves in Fig. 4 and 5 show an exponential curve. During this experiment the saturation level of the wetting phase reaches even a level that comes close to the irreducible saturation of this phase. This is one reason for the poor groundwater flow through the micromodel.

According to the relative permeability curve in Fig. 6 the wetting phase will even reach a relative permeability of almost 0 m². The positive effect of the hydrophobicity of the porous material on the relative permeability of the wetting phase (Beltrán et al., 2019) is not visible in the data of this study.

5.2.2 Experiment 2

The absence of air at the beginning of this experiment is an advantage in comparison with the first experiment. Due to this little happens during the first hours of the experiment. The incoming of a transparent suspension containing black (accumulations of) particles seems to be a mixture of groundwater with Nutrolase. They also seem to have formed while flowing through the tubes towards the micromodel.

Also for this experiment the pressure gradient across the porous medium decreases below 0 Pa at the first few hours. This is probably also due to the sensitivity of the pressure sensors which caused the same problem as for experiment 1. After an initial gradual decrease in pressure gradient, a sudden rise after about 2 hours occurs. Having a closer look at the images shows that at this time the black particles enter the micromodel that could have caused this small but sudden pressure gradient rise. Although the following pulses of black particles do not affect the pressure gradient furthermore until approximately after 4 hours. The sudden pressure gradient rise after about 4 hours interferes with the incoming air as seen from the images. From this point, the pressure gradient pattern continues at a more or less stable level around 2.5 kPa as the air keeps occupying the majority of the pore space. The most remarkable pressure gradient drops after 9 hours and 13 hours can be explained by the movement of air that creates space for some fluid to flow from the inlet to the outlet. Although these movements are relatively small on the entire scale, they create a pressure drop of 0.5-1 kPa.

It can be observed from the images that the dark particles suspended in the fluid flow are obviously coming from the inlet channels. Although it is not clear from the images of experiment 1 whether this is also the case. This can be due to the frequency of imaging (1 photo per 10 minutes) for the first experiment. This may have caused a lack in data that consequently caused to miss the origin of the particles. On the other hand, the frequency of experiment 2 was 1 photo per 30 seconds

causing to have a clearer view on the progress of the fluid and particle dynamics.

Also for this experiment the initial pressure data were not useful for the determination of the initial pressure gradient without clogging and therefore a reliable value for the clogging factor was not possible.

During the first hours of this experiment only a mixed fluid of groundwater and Nutrolase flows through the porous medium, in other words single-phase flow occurs. After 4 hours when the air phase enters the pore space multiphase flow should be considered. As initially no air is present in the pore space, a primary drainage curve shows the increase of the capillary pressure of the porous medium when the air enters the pore space (Fig. 4). This continues towards a value equivalent to a non-wetting phase saturation of about 60%. At the instances when some fluid flow pushes away some air the capillary pressure decreases for a moment. In Fig. 4 this is shown as the lines go from the main drainage curve towards the primary imbibition curve.

Also from this experiment can be observed that groundwater is the wetting phase due to the concave interface curvature of groundwater with the air phase.

5.3 CLSM images

As described and shown in the Theoretical background Section bacteria are generally at maximum a few μm in diameter. Moreover, the shape can differ from spherical to rod-shaped or spirally. The particles in the groundwater sample seem to be spherical but also too large to be bacteria. As these particles also did not show any movement, the likelihood for the existence of living bacteria in the groundwater ceased for this experiment. As different soil components also may be autofluorescent, it is more likely that these relatively large fluorescent particles are soil components other than bacteria. On the other hand, only 3 of the relative large particles seem to fluoresce. The other small red dots in the left bottom corner seem to be very small particles as large as 1 to a few μm large. So these are not the dark spots that can be more clearly seen at this part of the image, but smaller particles between them.

The addition of Fluoresbrite clearly shows (the abundance of) the components of both the groundwater and Nutrolase (Fig. 27a-c). Although the groundwater sample shows bright green spots in a matrix of many small green dots when excited with a 488 nm laser beam. The 405 nm laser beam does not excite the groundwater at all. On the other hand, a mixture of groundwater and Nutrolase with the fluorescent added shows the same particles enlighten for both laser beams. So from this observation it is not surely to say that the fluorescent particles are bacteria. But it can be stated that if bacteria are present in the groundwater, they do not reflect 405 nm wavelength light as this only occurs for particles in the Nutrolase fluid.

As these images were a trial to see what happens when adding fluorescent microspheres to the fluids, it might be probable that a too high volume of fluorescent suspension is added to the sample. This may cause the excess amount of the fluorescent microspheres to adsorb to other particles than bacteria.

6 Conclusions & Recommendations

Conclusions

This study started as a pilot experiment to observe how biosealing would occur at the pore scale. However it eventually ended up looking for evidence for the determination of the particles in the groundwater sample which is actually the basis for understanding the process at this scale.

By measuring the optical density at 600 nm of a groundwater sample, a cautious first proof for the presence of biological material can be given. Further analysis from observations of the groundwater below a confocal laser scanning microscope (CLSM) gives a more precise image of the presence and shape of certain particles in the groundwater. The addition of fluorescent microspheres causes these particles to fluoresce, but does not completely exclude the presence of other soil components as bacteria.

The results of this study show that bioclogging is a process that takes several days to clog a small artificial porous medium properly. The potential biomass visible in the micromodel experiments behaves dynamically as it moves around the pore space and end up along the boundary of the air phase. The first 4.5 hours of experiment 2 are the most reliable and useful as no air had yet entered the micromodel. This period shows at least that the 'biomass' gradually occupies the pore space, but needs more time to cause significant clogging in the absence of air. This is also stated by J.-W. Kim et al. (2010). Besides, the dark material has the tendency to enter the air when this is present in the pore space.

Injection of the fluids during experiment 2 with the open-microscope set-up is favourable over suction of the fluids into the micromodel. Suction causes the fluids to enter the micromodel with a delay, while this is not the case for injection. Also to saturate the pore space of the micromodel with water, initial injection with ethanol instead of CO₂ is also favourable as the pore space was saturated with water only when using ethanol.

Recommendations

As experienced during this study, a dynamic bioclogging experiment with a micromodel involves several factors that may influence the experiment unfavourably. Therefore it would be recommended to conduct a few static experiments involving the observations through time of a mixture of groundwater and Nutrolase using a confocal laser scanning microscope or even a Scanning Electron Microscope (SEM). A SEM is able to zoom even closer than a CLSM to the sample.

A significant improvement on the outcome of the micromodel experiments would be to find and solve the air leakage problem in the set-up. This had a major influence on the pressure measurements and could possibly be solved by putting silicone glue on all the parts where air may enter the system. Another recommendation would be to execute a more precise experiment with the spectrophotometer. In essence to measure the OD₆₀₀ of a groundwater sample with Nutrolase over a longer period of time to create a bacterial growth curve. This might give more insight in the presence and rate of growth of the bacterial population in the groundwater. Aside to this, a fluorescent dye, like Acridine Orange or DAPI, might be added to a groundwater sample and observed with the confocal microscope to have a more clear view on the presence of bacteria in the groundwater.

Some soil microbiological studies use a mixture of soil and groundwater from which the groundwater is extracted in the laboratory. As the majority of the bacteria are attached to soil grains, this

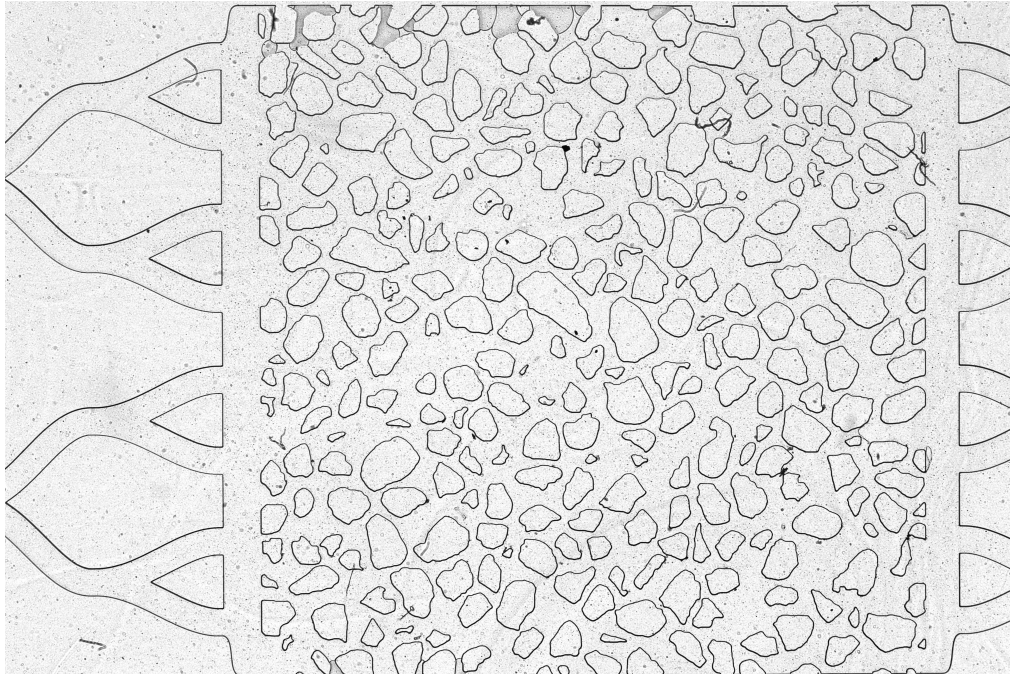
enables to have a more representative microbial community and a higher amount of bacteria in your groundwater sample.

When it is possible to clog the pore space with biomass in a micromodel, glass beads or other particles could be added to the system to simulate the flow and capturization of clay-like particles involved in the final steps of a BioSealing reaction.

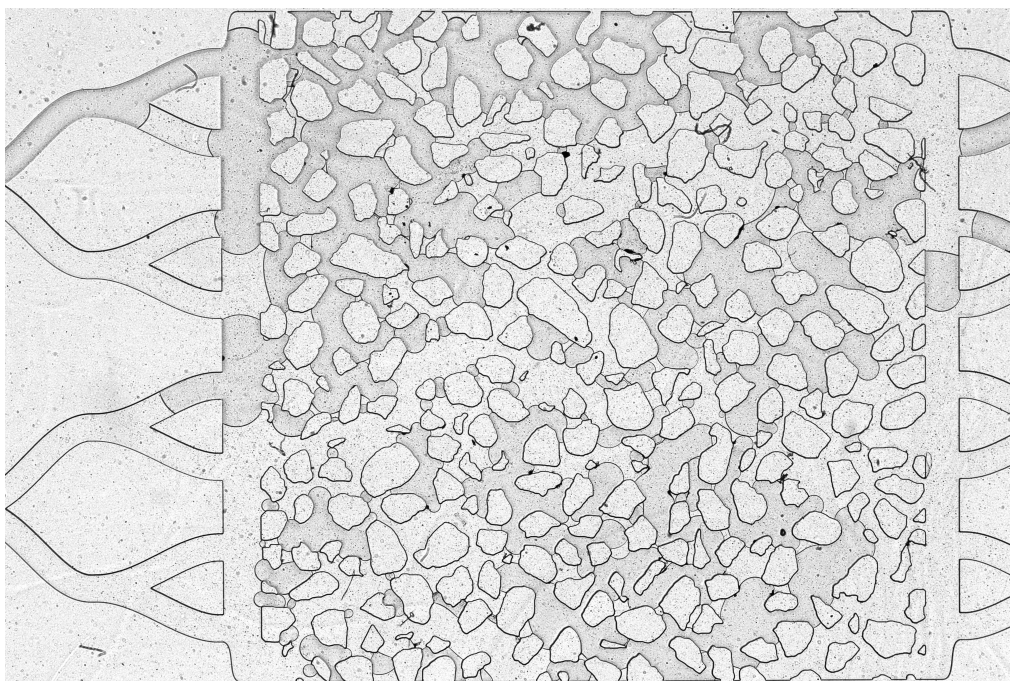
A Appendix

A.1 Images - Experiment 1 & 2

Experiment 1

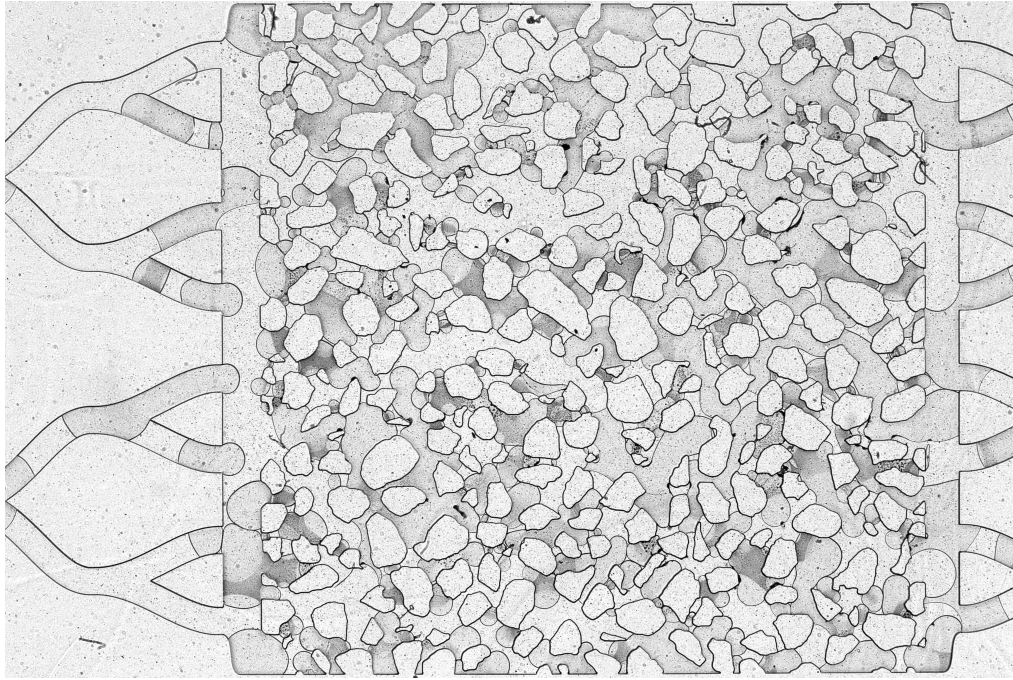


(a) $t=0$

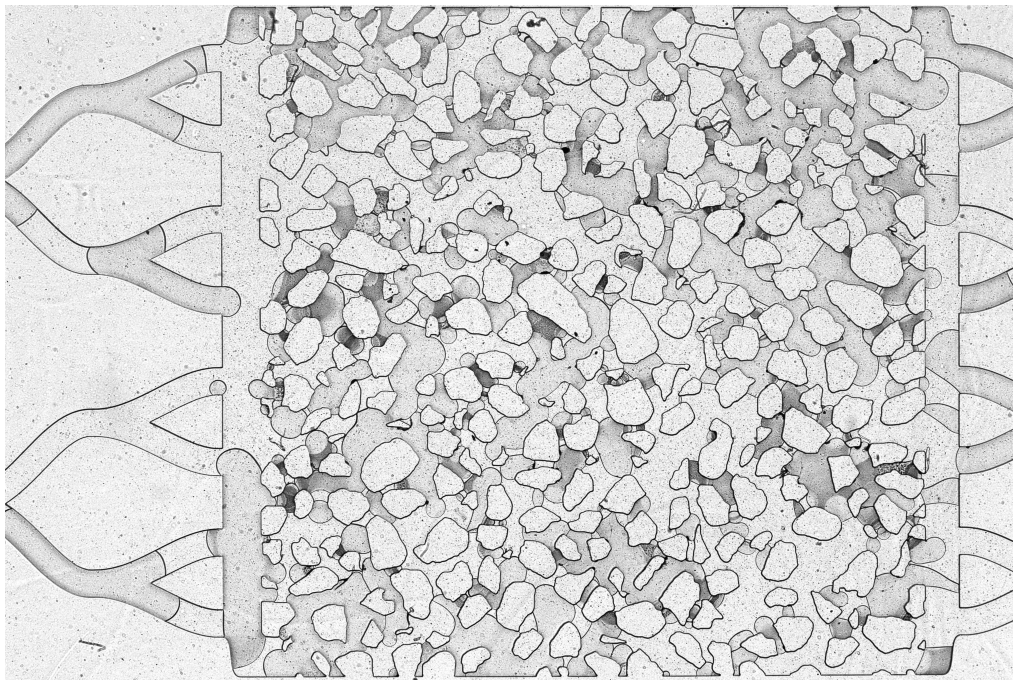


(b) $t=2.5$ hr

Figure 22: Experiment 1

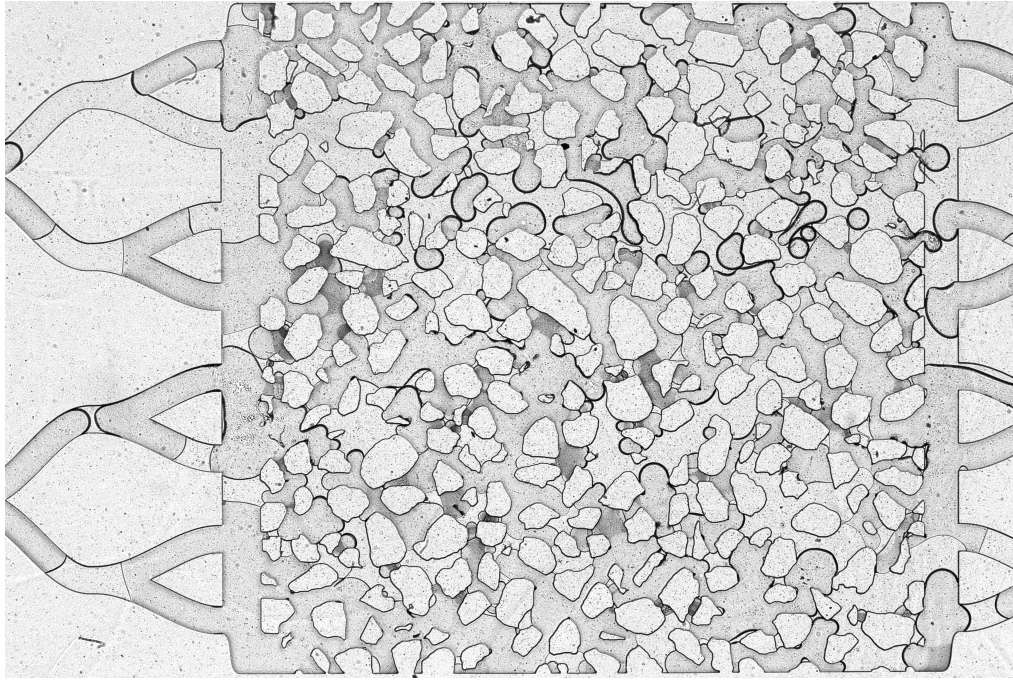


(c) $t=14.5$ hr

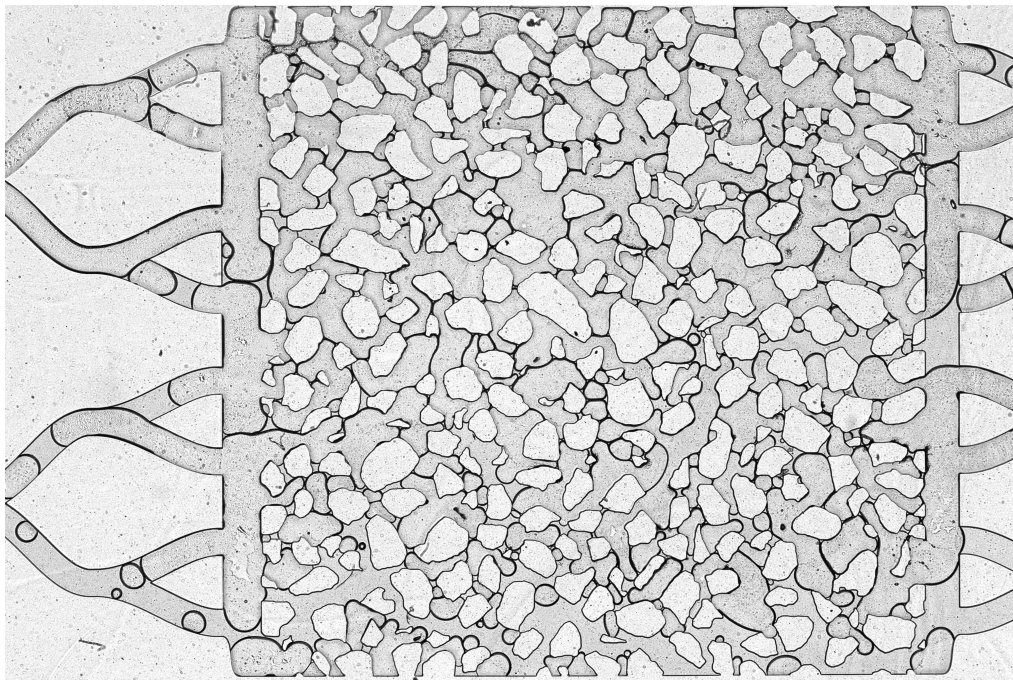


(d) $t=25$ hr

Figure 22: Experiment 1

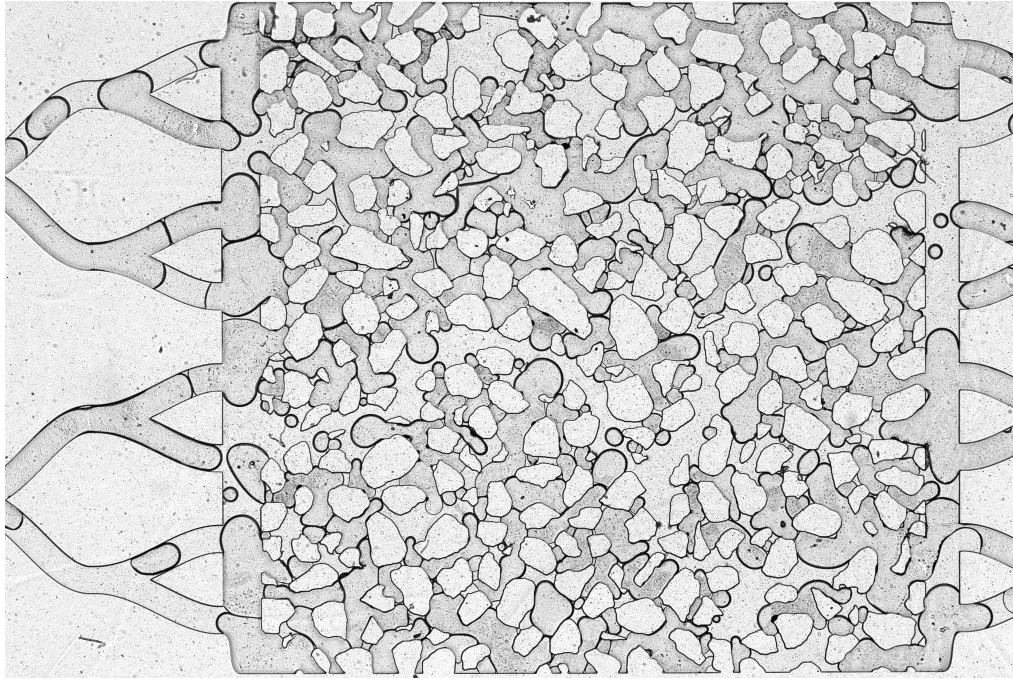


(e) $t=31.7$ hr



(f) $t=50$ hr

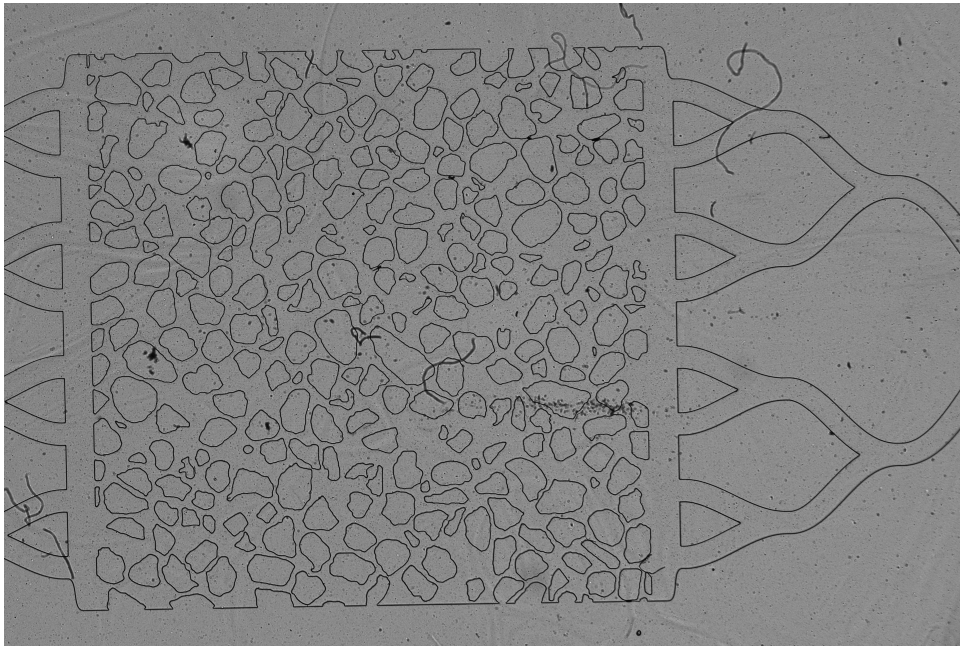
Figure 22: Experiment 1



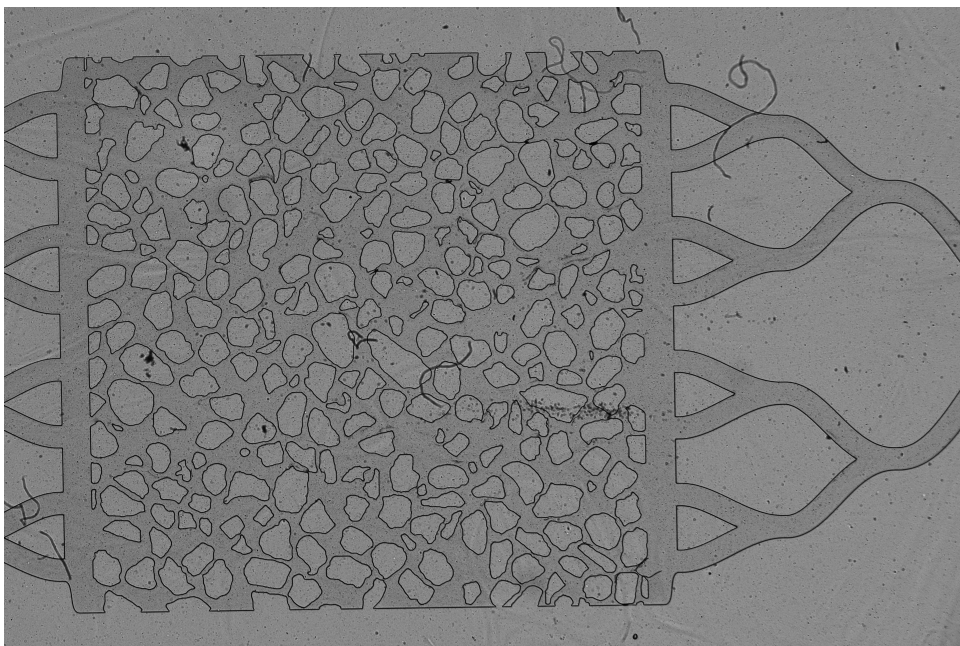
(g) $t=65$ hr

Figure 22: Experiment 1

Experiment 2

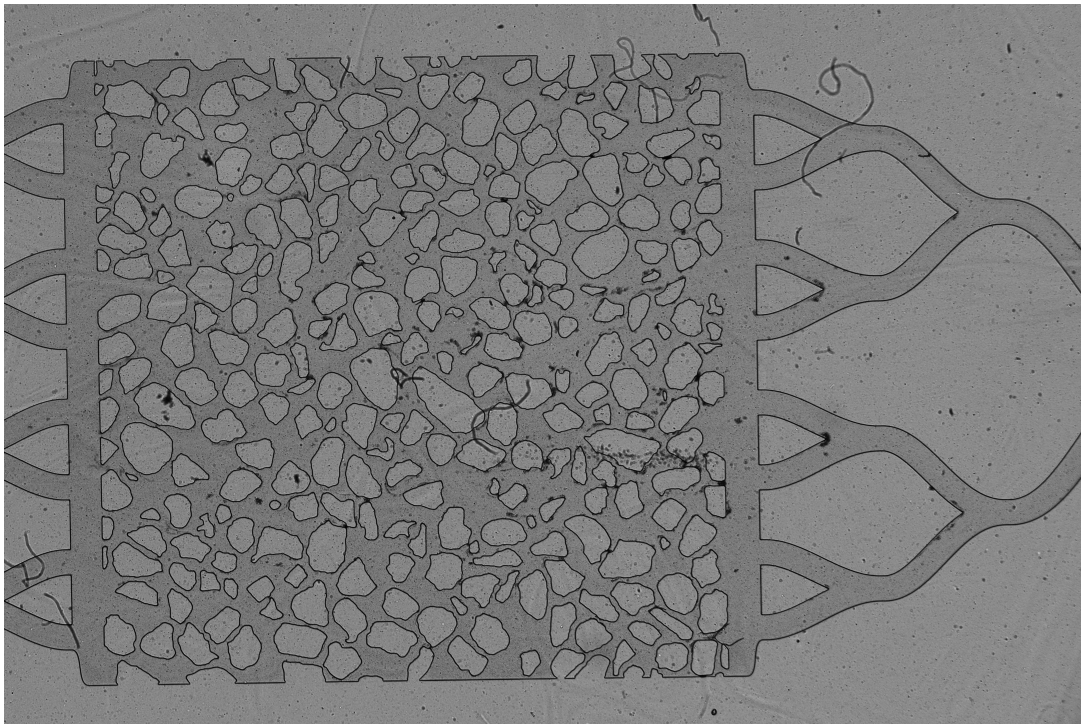


(a) $t=0$ hr

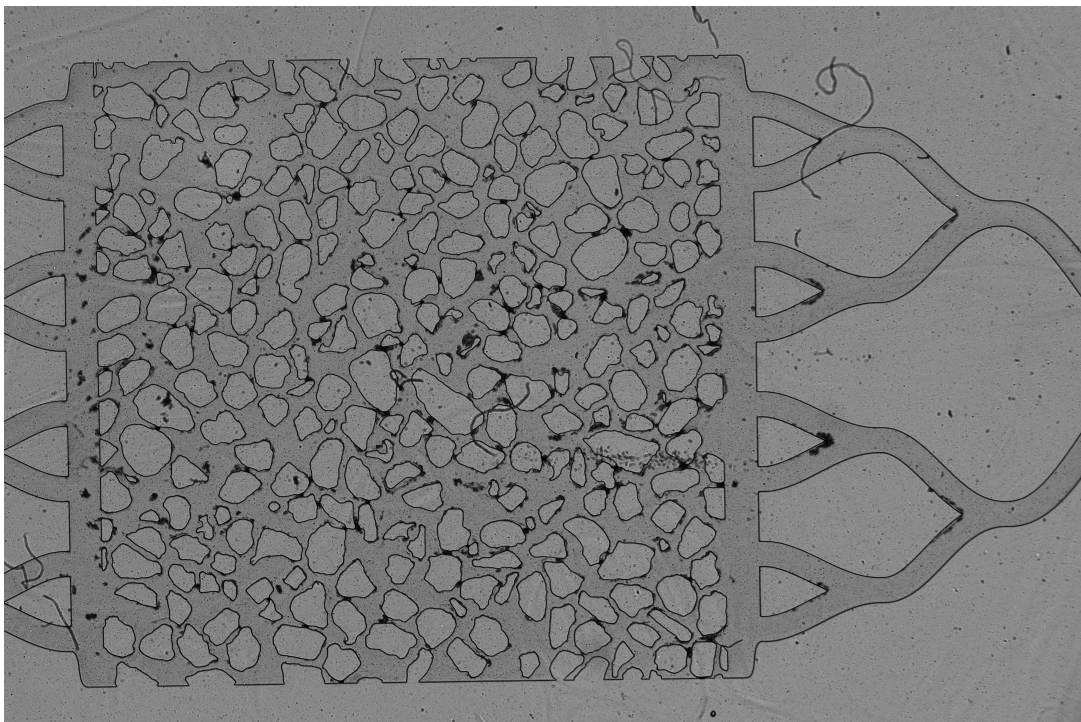


(b) $t=2.25$ hr

Figure 23: Experiment 2.

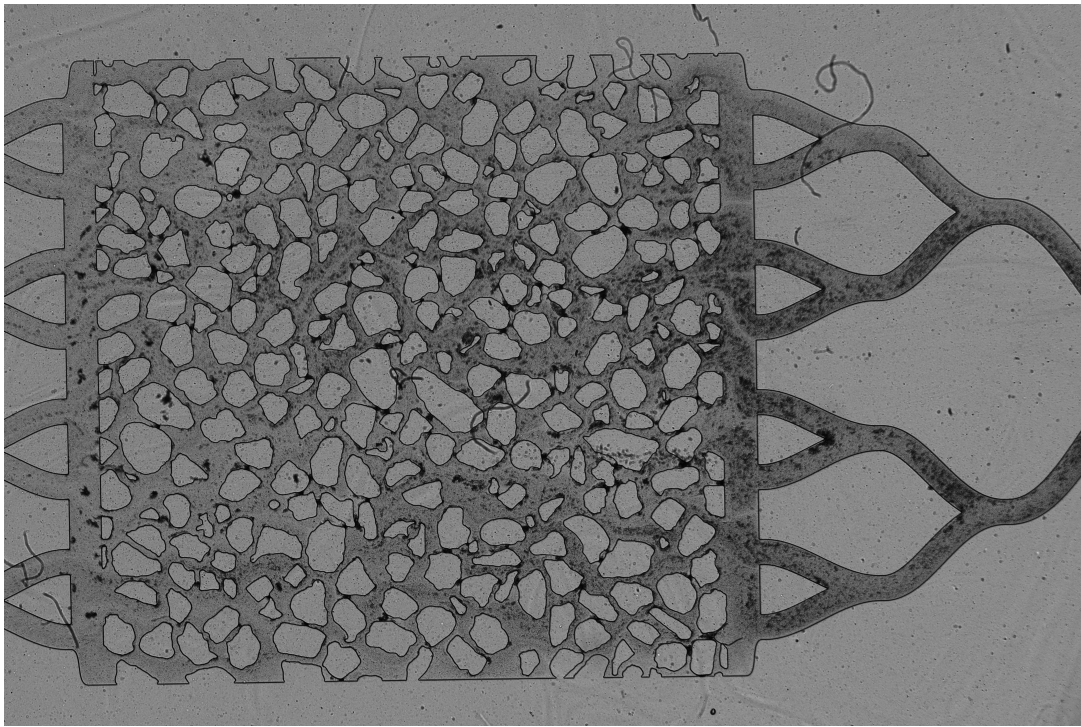


(c) $t=2.5$ hr

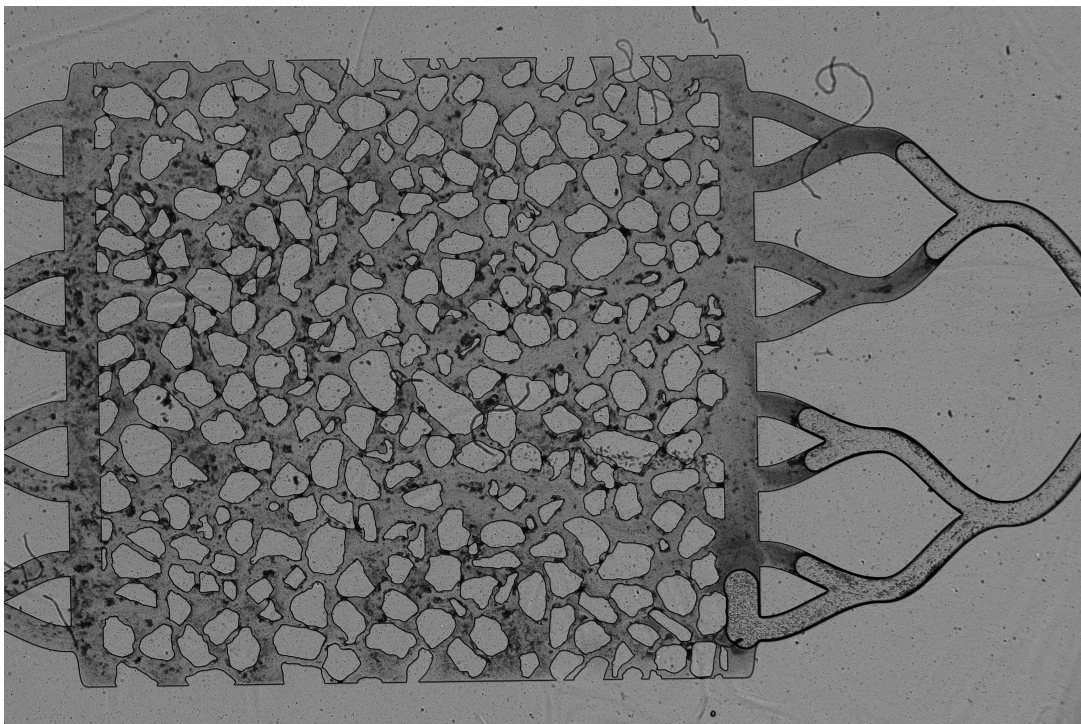


(d) $t=4.4$ hr

Figure 23: Experiment 2.

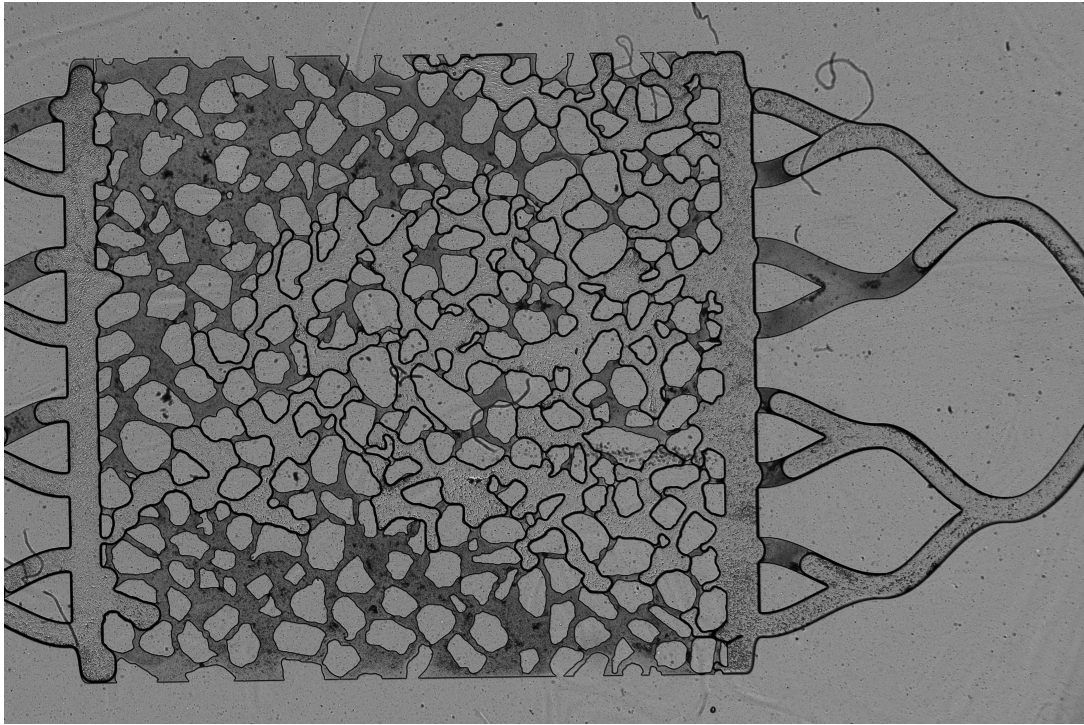


(e) $t=4.5$ hr

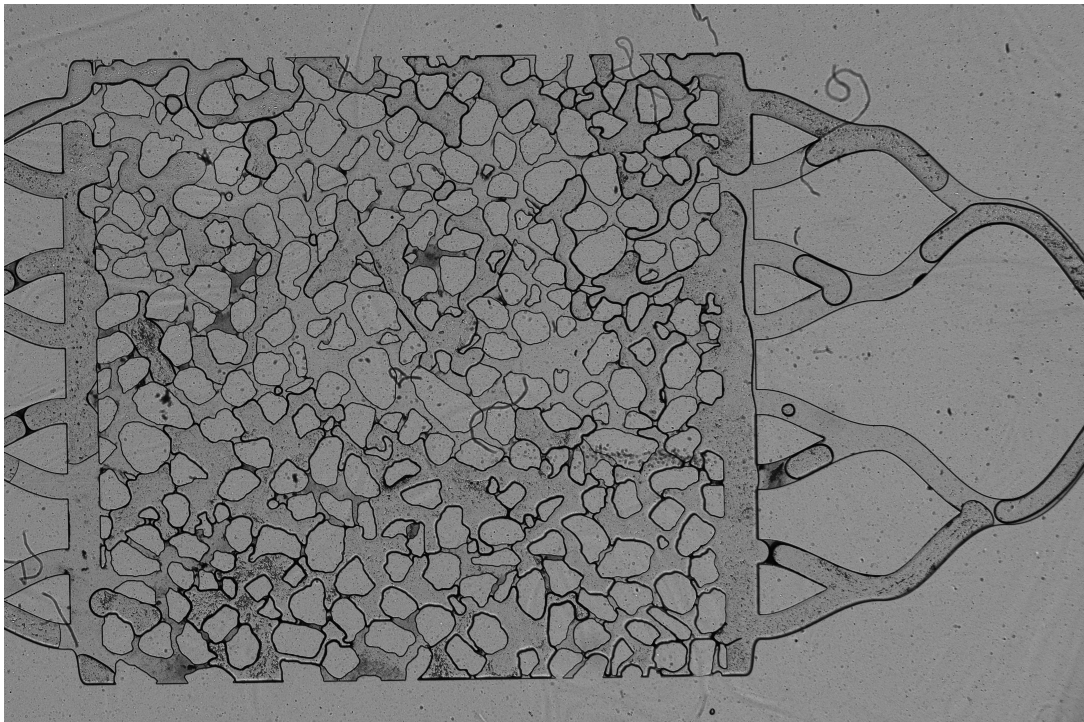


(f) $t=4.9$ hr

Figure 23: Experiment 2.



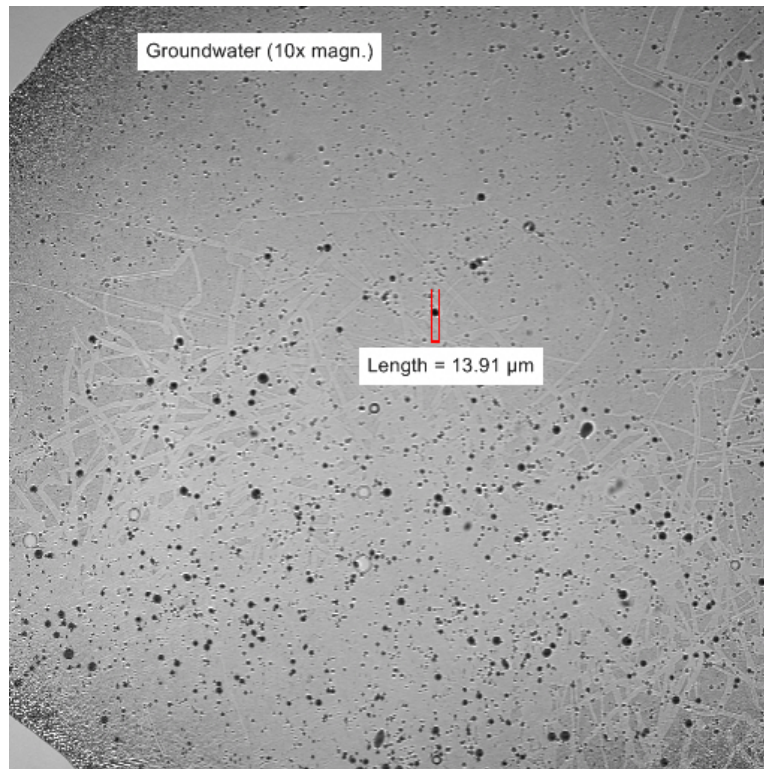
(g) $t=4.925$ hr



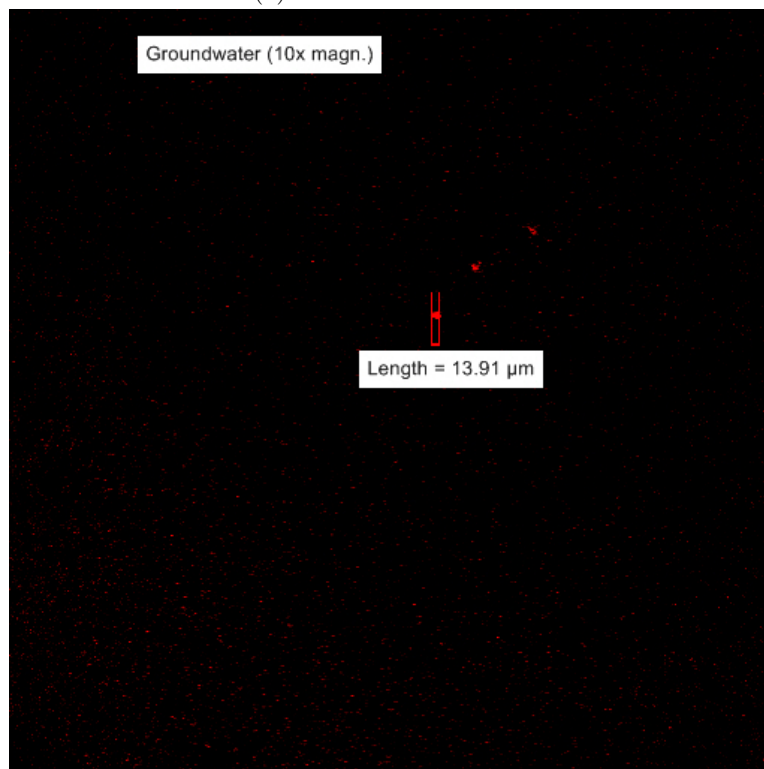
(h) $t=16.3$ hr

Figure 23: Experiment 2.

A.2 CLSM images

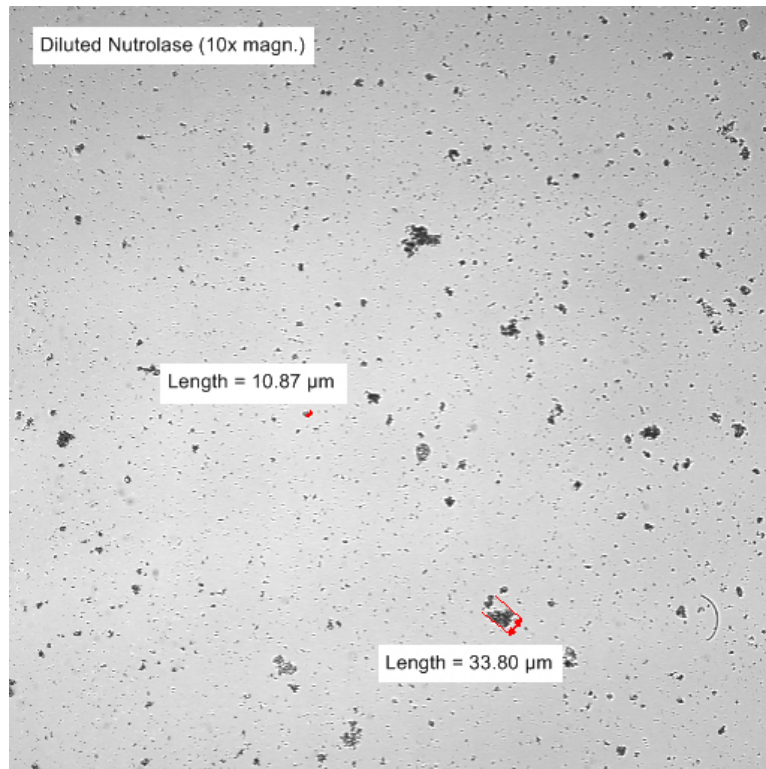


(a) Normal observation.

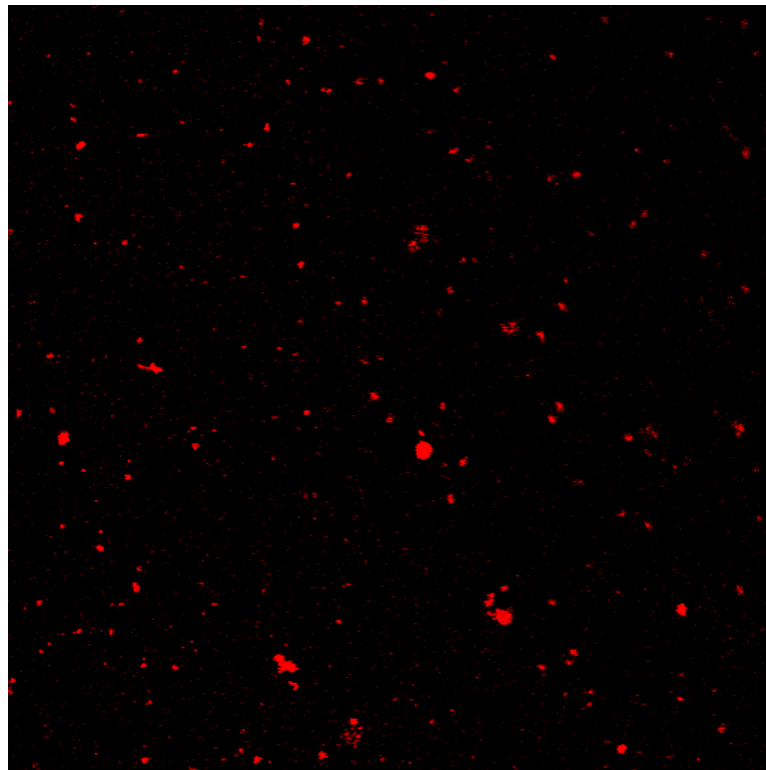


(b) Filtered observation (561 nm) without staining.

Figure 24: Groundwater.

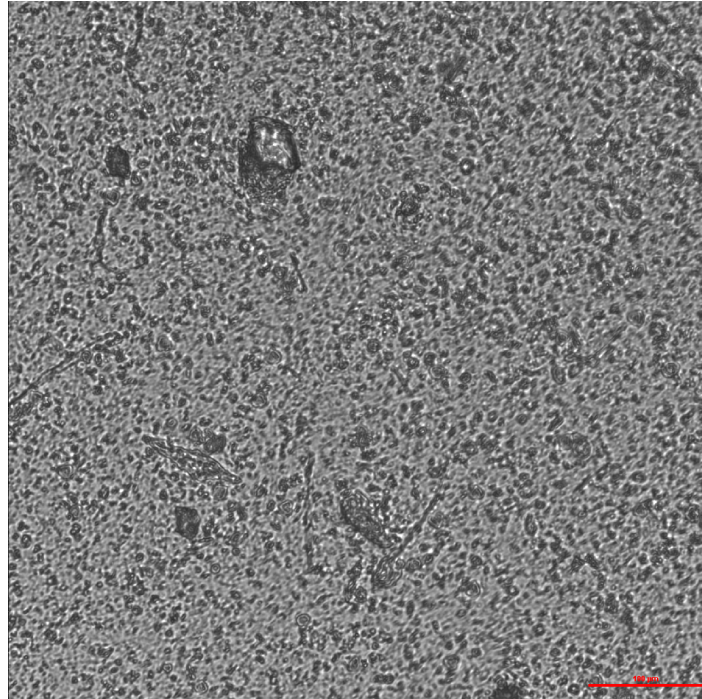


(a) Normal observation.

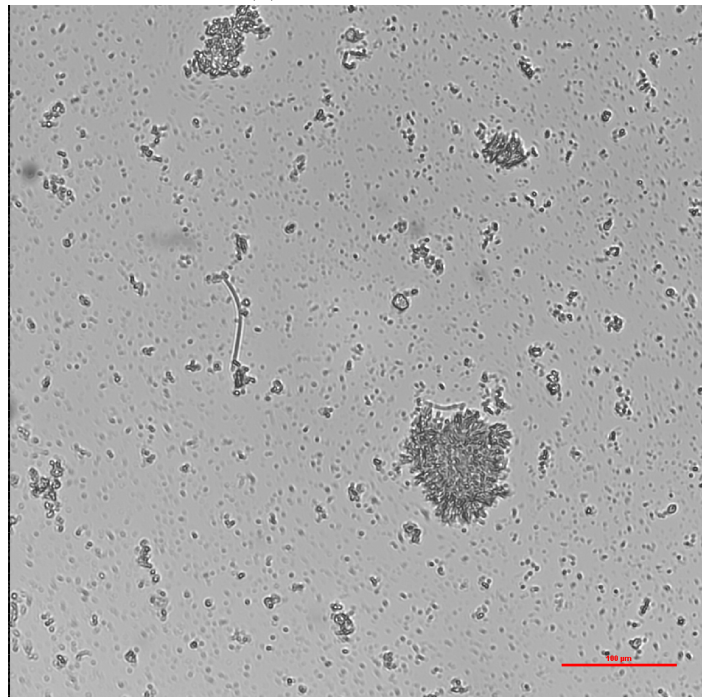


(b) Filtered observation (561 nm) without staining.

Figure 25: Diluted Nutrolase.

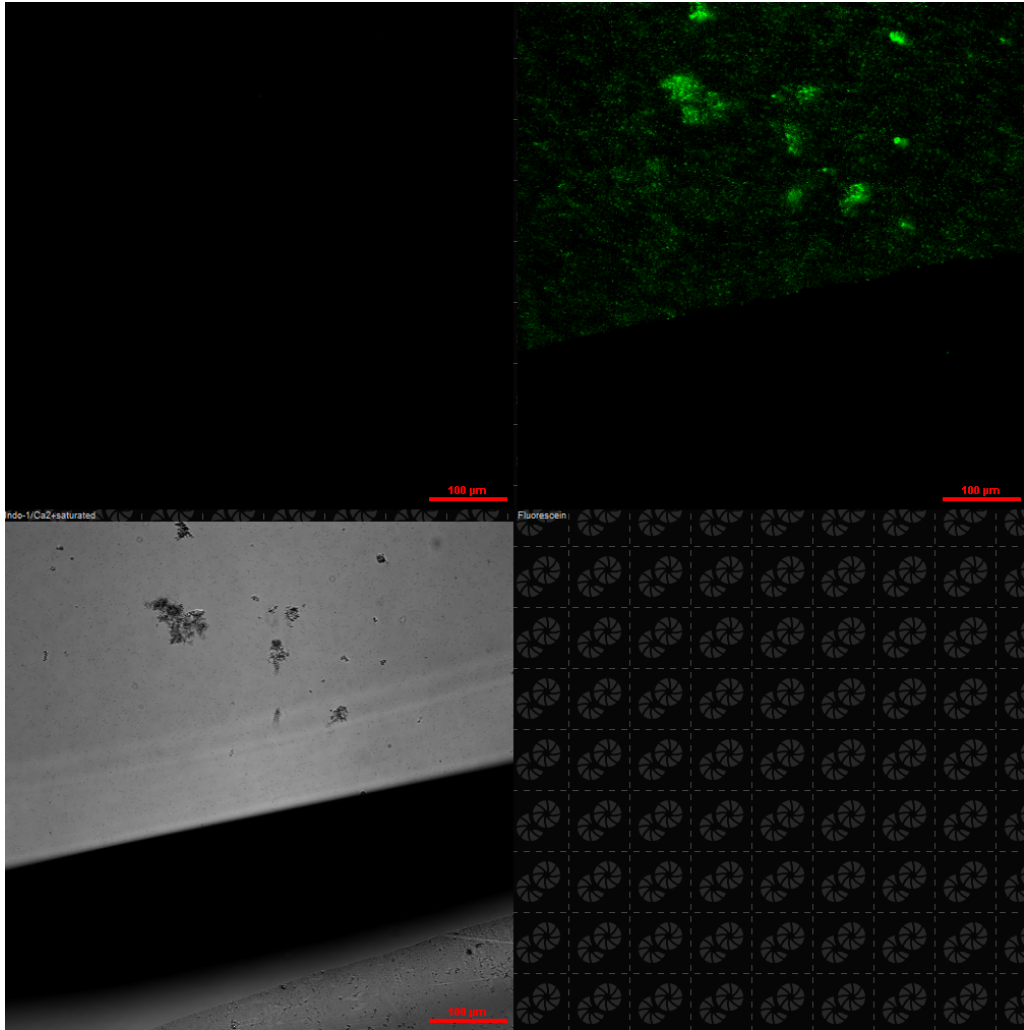


(a) Pure Nutrolase.



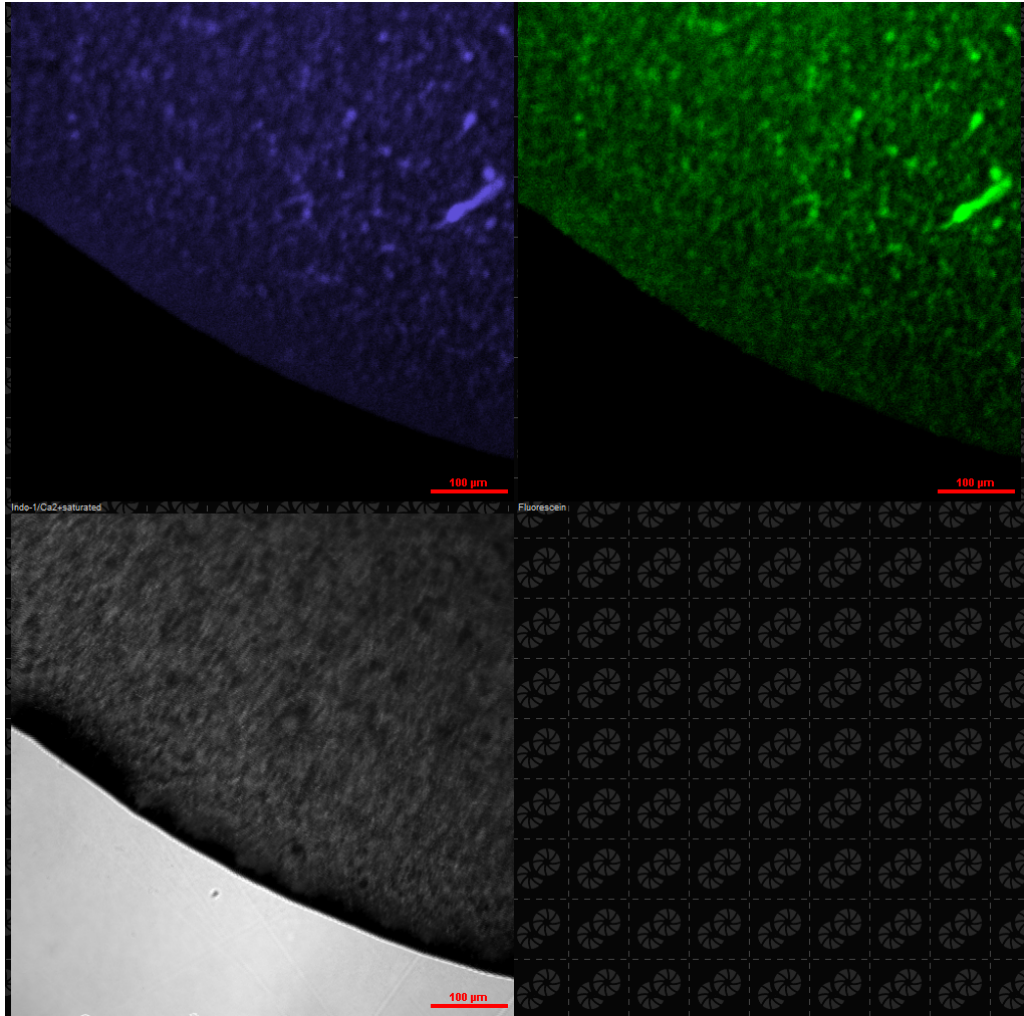
(b) Nutrolase diluted with groundwater.

Figure 26: Nutrolase



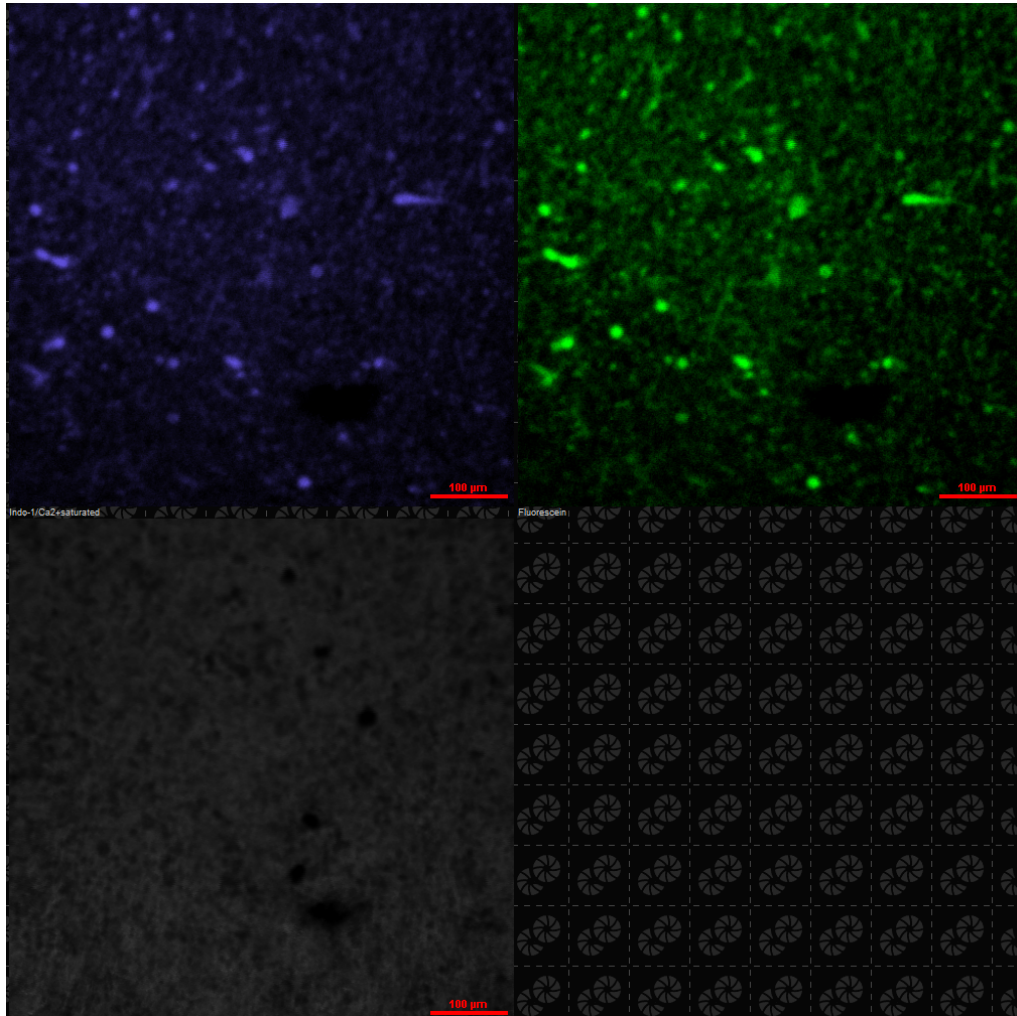
(a) Groundwater and Fluoresbrite.

Figure 27: Samples stained with fluoresbrite observed at 405 nm (top left image) and 488 nm (top right image). The left bottom image is a normal image.



(b) Groundwater, Nutrolase and Fluoresbrite.

Figure 27: Samples stained with fluoresbrite observed at 405 nm (topleft image) and 488 nm (topright image). The left bottom image is a normal image.



(c) Groundwater, Nutrolase and Fluoresbrite.

Figure 27: Samples stained with fluoresbrite observed at 405 nm (topleft image) and 488 nm (topright image). The left bottom image is a normal image.

References

- Abolmaaty, A., & Meyer, D. (2017). Pdms flow cell for monitoring bacterial adhesion capacity of escherichia coli o157: H7 in beverages. *Journal of Advances in Biology & Biotechnology*, 1–12.
- Avnimelech, Y., & Nevo, Z. (1964). Biological clogging of sands. *Soil Science*, 98(4), 222–226.
- Bao, N., Jagadeesan, B., Bhunia, A. K., Yao, Y., & Lu, C. (2008). Quantification of bacterial cells based on autofluorescence on a microfluidic platform. *Journal of Chromatography A*, 1181(1-2), 153–158.
- Bardgett, R. D., & Van Der Putten, W. H. (2014). Belowground biodiversity and ecosystem functioning. *Nature*, 515(7528), 505–511.
- Barton, A., Fullen, M., Mitchell, D., Hocking, T., Liu, L., Bo, Z. W., . . . Xia, Z. Y. (2004). Effects of soil conservation measures on erosion rates and crop productivity on subtropical ultisols in yunnan province, china. *Agriculture, Ecosystems & Environment*, 104(2), 343–357.
- Beltrán, A., Hernández-Díaz, D., Chávez, O., García, A., Mena, B., & Zenit, R. (2019). Experimental study of the effect of wettability on the relative permeability for air–water flow through porous media. *International Journal of Multiphase Flow*, 120, 103091.
- Blair, T. C., & McPherson, J. G. (1999). Grain-size and textural classification of coarse sedimentary particles. *Journal of Sedimentary Research*, 69(1), 6–19.
- Blauw, M., Lambert, J., & Latil, M.-N. (2009). Biosealing: a method for in situ sealing of leakages. In *Proceedings of the international symposium on ground improvement technologies and case histories, isgi* (Vol. 9, pp. 125–130).
- Chen, G., Zhang, Z., Guo, Q., Wang, X., & Wen, Q. (2019). Quantitative assessment of soil erosion based on csle and the 2010 national soil erosion survey at regional scale in yunnan province of china. *Sustainability*, 11(12), 3252.
- Delgado-Baquerizo, M., Oliverio, A. M., Brewer, T. E., Benavent-González, A., Eldridge, D. J., Bardgett, R. D., . . . Fierer, N. (2018). A global atlas of the dominant bacteria found in soil. *Science*, 359(6373), 320–325.
- Dupin, H. J., & McCarty, P. L. (2000). Impact of colony morphologies and disinfection on biological clogging in porous media. *Environmental science & technology*, 34(8), 1513–1520.
- Farah, T., Souli, H., Fleureau, J.-M., Kermouche, G., Fry, J.-J., Girard, B., . . . Harkes, M. (2016). Durability of bioclogging treatment of soils. *Journal of Geotechnical and Geoenvironmental Engineering*, 142(9), 04016040.
- Flemming, H.-C., & Wingender, J. (2010). The biofilm matrix. *Nature reviews microbiology*, 8(9), 623–633.
- Fuller, M. E., Streger, S. H., Rothmel, R. K., Mailloux, B. J., Hall, J. A., Onstott, T. C., . . . DeFlaun, M. F. (2000). Development of a vital fluorescent staining method for monitoring bacterial transport in subsurface environments. *Applied and Environmental Microbiology*, 66(10), 4486–4496.
- Hand, V. L., Lloyd, J. R., Vaughan, D. J., Wilkins, M. J., & Boulton, S. (2008). Experimental studies of the influence of grain size, oxygen availability and organic carbon availability on bioclogging in porous media. *Environmental science & technology*, 42(5), 1485–1491.

- Hockberger, P. E. (2000). The discovery of the damaging effect of sunlight on bacteria. *Journal of Photochemistry and Photobiology B: Biology*, 58(2-3), 185–191.
- Ivanov, V., & Chu, J. (2008). Applications of microorganisms to geotechnical engineering for bioclogging and biocementation of soil in situ. *Reviews in Environmental Science and Bio/Technology*, 7(2), 139–153.
- Kamel, F. H., Saeed, C. H., & Hassan, N. I. (2016). Comparative effect of different visible light energy on bacterial growth. *International Journal of Advanced Research*, 4(2), 263–270.
- Kapuscinski, J. (1995). Dapi: a dna-specific fluorescent probe. *Biotechnic & Histochemistry*, 70(5), 220–233.
- Karadimitriou, N., & Hassanizadeh, S. (2012). A review of micromodels and their use in two-phase flow studies. *Vadose Zone Journal*, 11(3), vzt2011–0072.
- Kim, D.-S., & Fogler, H. S. (2000). Biomass evolution in porous media and its effects on permeability under starvation conditions. *Biotechnology and Bioengineering*, 69(1), 47–56.
- Kim, J.-W., Choi, H., & Pachepsky, Y. A. (2010). Biofilm morphology as related to the porous media clogging. *Water Research*, 44(4), 1193–1201.
- King, L. K., & Parker, B. C. (1988). A simple, rapid method for enumerating total viable and metabolically active bacteria in groundwater. *Applied and environmental microbiology*, 54(6), 1630–1631.
- Leshchinsky, B., & Ambauen, S. (2015). Limit equilibrium and limit analysis: comparison of benchmark slope stability problems. *Journal of Geotechnical and Geoenvironmental Engineering*, 141(10), 04015043.
- Li, Y., Dick, W. A., & Tuovinen, O. H. (2003). Evaluation of fluorochromes for imaging bacteria in soil. *Soil Biology and Biochemistry*, 35(6), 737–744.
- Li, Y., Dick, W. A., & Tuovinen, O. H. (2004). Fluorescence microscopy for visualization of soil microorganisms—a review. *Biology and fertility of soils*, 39(5), 301–311.
- Liao, H., Zhao, K., Lambert, J., & Veenbergen, V. (2007). Experimental study on biosealing technology for seepage prevention. *age*, 1000(3).
- Maier, R. M., Pepper, I. L., & Gerba, C. P. (2009). *Environmental microbiology* (Vol. 397). Academic press.
- Mayer, A. S. (2005). *Soil and groundwater contamination: Nonaqueous phase liquids* (No. 17). American Geophysical Union.
- Orgiazzi, A., Bardgett, R. D., Barrios, E., et al. (2016). *Global soil biodiversity atlas*. European Commission.
- Pepper, I. L., & Gentry, T. J. (2015). Microorganisms found in the environment. In *Environmental microbiology* (pp. 9–36). Elsevier.
- Ren, J., Zhang, W., Wan, Y., Chen, Y., et al. (2017). Advances in the research of yunnan’s arid climate and extreme drought. *Atmospheric and Climate Sciences*, 7(01), 23.

- Roh, C., Lee, J., & Kang, C. (2016). Physical properties of pdms (polydimethylsiloxane) microfluidic devices on fluid behaviors: various diameters and shapes of periodically-embedded microstructures. *Materials*, *9*(10), 836.
- Ross, N., & Bickerton, G. (2002). Application of biobarriers for groundwater containment at fractured bedrock sites. *Remediation Journal*, *12*(3), 5–21.
- Ross, N., Novakowski, K. S., Lesage, S., Deschênes, L., & Samson, R. (2007). Development and resistance of a biofilm in a planar fracture during biostimulation, starvation, and varying flow conditions. *Journal of Environmental Engineering and Science*, *6*(4), 377–388.
- Sakamoto, C., Yamaguchi, N., & Nasu, M. (2005). Rapid and simple quantification of bacterial cells by using a microfluidic device. *Applied and environmental microbiology*, *71*(2), 1117–1121.
- Seifert, D., & Engesgaard, P. (2007). Use of tracer tests to investigate changes in flow and transport properties due to bioclogging of porous media. *Journal of contaminant hydrology*, *93*(1-4), 58–71.
- Semwogerere, D., & Weeks, E. R. (2005). Confocal microscopy. *Encyclopedia of biomaterials and biomedical engineering*, *23*, 1–10.
- Stoodley, P., Sauer, K., Davies, D. G., & Costerton, J. W. (2002). Biofilms as complex differentiated communities. *Annual Reviews in Microbiology*, *56*(1), 187–209.
- Suresh Kumar, A., Mody, K., & Jha, B. (2007). Bacterial exopolysaccharides—a perception. *Journal of basic microbiology*, *47*(2), 103–117.
- Thullner, M., Mauclaire, L., Schroth, M. H., Kinzelbach, W., & Zeyer, J. (2002). Interaction between water flow and spatial distribution of microbial growth in a two-dimensional flow field in saturated porous media. *Journal of contaminant hydrology*, *58*(3-4), 169–189.
- Valiei, A. (2013). Biofilm streamer formation in a porous microfluidic device.
- Van Beek, V., Den Hamer, D., Lambert, J., Latil, M., & Van Der Zon, W. (2007). Biosealing, a natural sealing mechanism that locates and repairs leaks. In *Proceedings of the 1th international conference on self healing materials, noordwijk aan zee, the netherlands* (pp. 18–20).
- van der Zon, W. H., Den Hamer, D. A., Lambert, J. W. M., & olaf Molendijk, W. (2012, September 4). *Biosealing*. Google Patents. (US Patent 8,256,994)
- Vandevivere, P., & Baveye, P. (1992). Saturated hydraulic conductivity reduction caused by aerobic bacteria in sand columns. *Soil Science Society of America Journal*, *56*(1), 1–13.
- Vermeulen, N., Keeler, W. J., Nandakumar, K., & Leung, K. T. (2008). The bactericidal effect of ultraviolet and visible light on escherichia coli. *Biotechnology and bioengineering*, *99*(3), 550–556.